# On tangent geometry and generalised continuum with defects

van Hoi Nguyen, Guy Casale, Loïc Le Marrec

# On tangent geometry and generalised continuum with defects

Van Hoi Nguyen , Guy Casale and Loïc Le Marrec Univ Rennes, CNRS, IRMAR-UMR 6625, Rennes, France

This paper introduces tools on fibre geometry towards the framework of mechanics of microstructured continuum. The material is modelled by an appropriate bundle for which the associated connection and metric are induced from the Euclidean space by a smooth transformation represented by a fibre morphism from the bundle to Euclidean space. Furthermore, the general kinematic structure of the theory includes macroscopic and microscopic fields in a multiscaled approach, including large transformation. Defects appear in this geometrical point of view by an induced curvature, torsion and non-metricity tensor in the induced geometry. Special attention is given to transport along a finite path in order to extend the standard infinitesimal analysis of torsion and curvature to a macroscopical point of view. Both theoretical and numerical analysis may be handled without additional difficulties. Accordingly, several examples of transformation involving the distribution of material defects are exhibited and analysed.

**Keywords**
Riemann–Cartan geometry, Weyl manifold, fibre bundle, Ehresmann connection, defective media, microstructure, curvature, torsion, non-metricity tensor

## 1. Introduction

A hundred years ago, Cartan exposed the overall properties of the so-called Riemann–Cartan (RC) manifold endowed with not only a Riemannian metric (measuring the shape change) but also an affine connection incorporating torsion and curvature in the geometrical problem [1]. In this seminal note, the mathematical techniques are not present (it contains no equations), but the author insists on the crucial interpretation of lack of closure supported by a moving frame after a parallel transport along an infinitesimal loop. Interestingly, the paper is devoted to modelling of a *material continuum* containing infinitesimal *universe* and particular attention is paid to mechanical concepts such as *energy*, *equilibrium*, *forces* and *torques*. The paper was inspired by the Cosserat brothers who introduced a continuum model involving an independent field of rotation in addition to the standard displacement field [2]. From a crystalline point of view, the Cartan's approach is known as closely related to the work of Burgers brothers [3] even if these latter were more inspired by Volterra's ideas (on continuum) [4]. From a geometrical point of view Cartan's inspiration takes its roots in the general relativity and especially on the Weyl's 1918 works in which the author introduced an independence between the affine connection and metric tensor [5]. Cartan published a series of articles [6–8], where he presented a theory of generalised relativity in the framework of his formulation of affine geometry. If the geometrical concepts are defined in these works, there is no more reference to material continuum as it was sketched in the first note of 1922.

Since the 1950s, the close link between continuum mechanics of solids with a distribution of defect and RC geometry has been re-activated by Kondo [9], and independently by Bilby, Bullough, and Smith [10]. These seminal works made the identification of the Cartan circuit with the Burgers circuit, and with the torsion tensor being interpreted as the dislocation density. Later, Kröner [11, 12] highlighted that the Riemannian circuit brings a perspective for modelling distributions of disclinations in a continuum. In other words, curvature tensor is identified with disclination density. Hence, disclinations are the rotational counterpart of dislocations (translational defects) [13]. Application to initially crystalline defects has been extended progressively to defects in (inhomogeneous) material through more general mathematical supports [12, 14–16].

Among the applications, the elastoplasticity of solids is one of themes most concerned by these approaches. Indeed, physical considerations of such mechanisms associate the notion of a micro-structure within the solid together with a notion of defects capable of flowing through the material structure. For finite elastoplastic deformation, the total deformation tensor is generally decomposed multiplicatively into an elastic and plastic part $\mathbb{F} = \mathbb{F}_e\mathbb{F}_p$, which was originally proposed in [10, 11] and [17]. Here $\mathbb{F}_p$ represents the plastic distortion due to the flow of defects through the material structure, whereas $\mathbb{F}_e$ is the local deformation due to the stretch and rotation of the material structure. Note that $\mathbb{F}_e$ and $\mathbb{F}_p$ are not defined as the gradients of a continuous one-to-one mapping, see [18]. From a heuristic point of view, this decomposition introduces an intermediate configuration: $\mathbb{F}_p$ may be interpreted as a local deformation from the initial configuration to an intermediate one, whereas $\mathbb{F}_e$ relates the intermediate state to the current configuration. However, such decomposition may be recovered without invoking an intermediate configuration, but by a homogenisation process [19] or by invoking geometrical models [20].

Another well-known approach consists of focusing on the discontinuity of scalar and vectorial fields [15] by invoking multivalued fields [21]. Such an approach is a microscopic alternative interpretation of the non-holonomy supported by geometrical quantities (scalar or tensorial) at a scale for which the material may be interpreted as a continuum [22]. Even if this approach was inspired by the elastoplastic transformation of crystals, its applications have a wider range including relativity and quantum mechanics [13, 23]. In this modelling, the global $\mathscr{C}^1$-regular embedding is replaced by a multivalued map and, hence, the global coordinate transformation is replaced by a local one $dx^a = \mathbf{e}^a_A\, dX^A$. Such maps carry flat space to space with curvature and torsion. It is therefore usual to define connection coefficients as extension of the usual definition $\widehat{\Gamma}^A_{BC} = \mathbf{e}^A_c \partial_B \mathbf{e}^c_C$ and the metric $\widehat{\mathbf{G}}_{AB} = \mathbf{e}^a_A \mathbf{g}_{ab} \mathbf{e}^b_B$. The connection is metric compatible. Torsion of the connection may be introduced explicitly [24, 25] or via a distortion field [26]. Even if multivaluation of some fields may introduce some difficulties, numerical simulations can be performed and lead to applications in solid and fluid mechanics [27].

In linear elasticity, micromorphic theory [28, 29] extends the couple-stresses theory of Mindlin [30]. Following the paradigm of the Cosserat brothers, attention is mainly given to a new degree of freedom illustrating the versatility of microstructured media. Nowadays, the size effects involved in a natural way in this model have received increased attention both in statics [31–33] and dynamics [34–36]. Even if micromorphic theories share mainly the same overall objective as the other formulation, extension to large transformation is at this stage not completely elucidated [37]. One of the possible reasons is that this theory is constructed on a restrictive geometrical formulation. The present paper is a contribution in this direction among recent works [22, 38–40].

Indeed a microcontinuum can be modelled as a fibre bundle because it suffices to mention that each point on the base manifold can be considered endowed with additional degrees of freedom or internal variables. In this context, the motion of the microcontinuum is formally a fibre morphism [41]. In fibre bundle geometry, geometric objects such as metric tensors [42], connections and derived quantities (torsion, curvature) may depend not only on position but also on the internal state [43]. This extends the Riemannian geometry for which (relative) position of material points controls all geometrical objects as underlined by [5]. Fibre geometry encompasses various geometries among Euclidean, Riemannian, Weitzenböck and Weyl manifolds. Its application concerns mainly the general relativity but other applications have already been investigated [44, 45]. As such approach considers the macroscopical and microscopical universes as a whole, all the physical quantities may be considered as single-valued and smooth (outside macroscopical inhomogeneities). Accordingly, both theoretical and numerical analysis may be handled without additional difficulties.

This paper is organised as follows. Section 2 is devoted to the concepts of the geometrical formulation of a microstructured continuum $\mathscr{M}$ where a solder form, an Ehresmann connection and a (Sasaki) metric are defined on a fibre bundle. These concepts are essential ingredients in this paper. In Section 3 these notions are applied to material transformations. As the primary intention is to describe structural changes in real materials, special attention is paid to kinematical interpretation. In this context, a *scaled material modelling* is introduced. This model is devoted to material transformations represented by fibre morphisms. Accordingly, induced connection

and metric are first described, then driven geometrical quantities such as curvature, torsion, and non-metricity tensor are obtained. In Section 4, alternative approaches are reviewed and compared, significant features of the proposed model are also exhibited. The applications of this theory are presented in Section 5. Dedicated simulations are provided for each process and in various description's spaces (tangent space, body, etc). Then several examples of material transformation with distributed defects are proposed and discussed. Conclusions follow in Section 6. At the end, an appendix contains a brief reminder of RC geometry and details of some proofs.

## 2. Geometrical background

A microstructured material is modelled by a fibre bundle $\mathscr{M} \xrightarrow{\pi} \mathscr{B}$ with extra data described in this section. The three-dimensional differentiable manifold $\mathscr{B}$ is compact with boundary and orientable. It is the geometrical locus of the material, hereafter called the *body*. The fibre of the bundle $\mathscr{M}$ at $p \in \mathscr{B}$ is denoted by $\mathscr{M}_p$. It is considered as the microelement constituent of the material at the point $p$.

After the general definitions, each subsection will end with the application of the definition in a special case where the tangent bundle $\mathscr{M}$ is $T\mathscr{B}$. Indeed $\mathscr{M} = T\mathscr{B}$ means that microelements are interpreted as a first-order infinitesimal neighbourhood of geometrical points. Such interpretation coincides with standard analysis with defective crystals or grained material. This equality means that the same mathematical object, namely $T\mathscr{B}$, is used to model different mechanical objects: the space of "speed" of geometrical point $p : T_p\mathscr{B}$ on the one hand and the microelement at $p : \mathscr{M}_p$ on the other hand.

This general formalism, supposing that eventually $\mathscr{M} \neq T\mathscr{B}$, has also the advantage of extending the present theoretical background to other physical materials (porous media, phase transformation, soft matter, etc.; see, for example, [46–48]).

### 2.1. Solder form

Let us denote by $V(\mathscr{M})$ the vertical tangent bundle of $\mathscr{M} \xrightarrow{\pi} \mathscr{B}$, i.e. the subbundle $\ker d\pi \subset T\mathscr{M}$. The fibre of $V(\mathscr{M})$ at $p \in \mathscr{B}$ is the tangent bundle to the microelement $\mathscr{M}_p$, namely $T(\mathscr{M}_p)$. One considers that the tangent at the microelement at $m \in \mathscr{M}_p$, namely $T_m(\mathscr{M}_p) \equiv V_m\mathscr{M}$, should be $T_p\mathscr{B}$, meaning that microelements are tangent to the body $\mathscr{B}$. It is formalised in the following definition.

**Definition 2.1.** *A solder form on $\mathscr{M}$ is an isomorphism $T\mathscr{B} \underset{\mathscr{B}}{\times} \mathscr{M} \xrightarrow{\vartheta} V(\mathscr{M})$.*

The definition (2.1) implies that the dimension of a microelement is equal to the dimension of $\mathscr{B}$. Hereafter, we consider the case where $\dim \mathscr{B} = \dim \mathscr{M}_p$. An alternative definition of the solder form can be found in [49].

Let $(x^a)$ be coordinates on $\mathscr{B}$ and let them be complete in a coordinate system $(x^a, y^i)$ on $\mathscr{M}$. A solder form can be written accordingly:

$$\vartheta = \vartheta^i_a(m)\frac{\partial}{\partial y^i} \otimes dx^a.$$

If $\widetilde{x}^a(x^b)$ and $\widetilde{y}^i(x^b, y^j)$ defines another coordinate system on the bundle $\mathscr{M}$, then we have

$$\vartheta = \widetilde{\vartheta}^i_a(m)\frac{\partial}{\partial \widetilde{y}^i} \otimes d\widetilde{x}^a = \left(\widetilde{\vartheta}^i_a(m)\frac{\partial y^j}{\partial \widetilde{y}^i}\frac{\partial \widetilde{x}^a}{\partial x^b}\right)\frac{\partial}{\partial y^j} \otimes dx^b.$$

When $\mathscr{M}$ is a vector bundle on $\mathscr{B}$, then one has $V(\mathscr{M}) = \mathscr{M} \underset{\mathscr{B}}{\times} \mathscr{M}$. A particular type of solder form can be defined by a bundle map over $\mathscr{M}$, $T\mathscr{B} \underset{\mathscr{B}}{\times} \mathscr{M} \xrightarrow{\vartheta} \mathscr{M} \underset{\mathscr{B}}{\times} \mathscr{M}$, induced by an isomorphism $T\mathscr{B} \to \mathscr{M}$. This is a strong interpretation of the tangency condition of $V(\mathscr{M})$ with $\mathscr{B}$ modelled by the solder form.

One should keep in mind that the bundle $T\mathscr{B}$ is used to model two different objects: the tangent spaces $T\mathscr{B}$ on the one hand, and the microelements $\mathscr{M}$ on the other hand.

For the special case $\mathscr{M} = T\mathscr{B}$, the canonical solder form is reduced to the isomorphism associated to the identity $T\mathscr{B} = \mathscr{M}$. This isomorphism $T\mathscr{B} \underset{\mathscr{B}}{\times} \mathscr{M} \xrightarrow{\vartheta_{can}} V(\mathscr{M})$ is given by the following construction. A coordinate

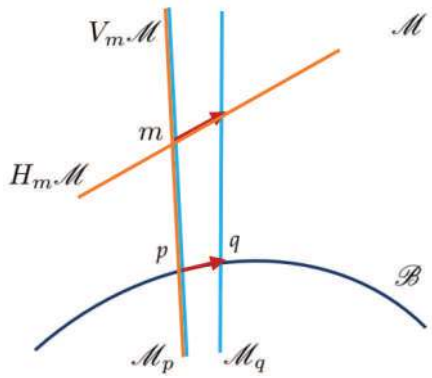


**Figure 1.** Pictorial representation of the Ehresmann connection.

system $(x^a)$ on $\mathscr{B}$ induces coordinates $(x^a, y^i)$ on $T\mathscr{B}$ such that for $v \in T\mathscr{B}$, $v = \delta^a_i y^i(v)\dfrac{\partial}{\partial x^a}$. Expressed with these coordinates, the canonical solder form is

$$\vartheta_{can} = \delta^j_b \frac{\partial}{\partial y^j} \otimes dx^b.$$

## 2.2. Connections

For infinitesimally closed points $p$ and $q$ in $\mathscr{B}$, the identification of the microelements $\mathscr{M}_p$ and $\mathscr{M}_q$ is a matter of choice that takes part to the overall model. This identification is performed by using a field of tangent vector to $\mathscr{M}$ along $\mathscr{M}_p$ whose projection on $\mathscr{B}$ is the constant vector $\vec{pq}$. This should be done along any fiber $\mathscr{M}_p$ and this assignment should be smooth and unique. This task is performed by Ehresmann connections (Figure 1).

**Definition 2.2.** *An Ehresmann connection on $\mathscr{M}$ is a morphism $N : T\mathscr{B} \underset{\mathscr{B}}{\times} \mathscr{M} \to T\mathscr{M}$ such that $d\pi \circ N(v, m) = v$. In local coordinates $(x^a, y^i)$,*

$$N = \left(\frac{\partial}{\partial x^a} - N^i_a(m)\frac{\partial}{\partial y^i}\right) \otimes dx^a.$$

This formula could be interpreted as follows: the microelement $\mathscr{M}_p$ at $p$ (with coordinates $(x^a)$) is identified with its neighbour $\mathscr{M}_q$ at $q$ (with coordinates $(x^a + dx^a)$) using the infinitesimal transformation $\left(-N^i_a(m)dx^a\right)\dfrac{\partial}{\partial y^i}$ where $m \in T_p\mathscr{M}$. If points $p$ and $q$ are connected by a finite path $\sigma$, then $\mathscr{M}_q$ is identified with $\mathscr{M}_p$ by solving $(dy^i + N^i_a(m)dx^a)|_\sigma = 0$ with $m = (x, y)$. This last ordinary differential equation (ODE) may not have a solution defined on the whole path $\sigma$ and then the finite identification may not exist. A large class of connections ensuring the existence of finite identification is given by principal connections. Among them, the linear and affine connections are described in the following.

Equivalently, the Ehresmann connection consists of a smooth assignment to each point $m \in \mathscr{M}$ of a supplementary subspace, the horizontal subspace $H_m\mathscr{M} \subset T_m\mathscr{M}$ to the vertical subspace of the tangent bundle of $V_m(\mathscr{M}) \subset T_m\mathscr{M}$. We can lift the natural local basis $\partial/\partial x^a$ of $T_p\mathscr{B}$ to respective bases of the horizontal space at any point $m \in \mathscr{M}_p$ and, hence,

$$H_m\mathscr{M} = \text{span}\left(\frac{\delta}{\delta x^a} = \frac{\partial}{\partial x^a} - N^i_a(m)\frac{\partial}{\partial y^i}\right) \qquad \text{and} \qquad V_m\mathscr{M} = \text{span}\left(\frac{\partial}{\partial y^i}\right). \tag{1}$$

The dual of the horizontal and vertical tangent spaces are given by

$$H^*_m\mathscr{M} = \text{span}(dx^a) \qquad \text{and} \qquad V^*_m\mathscr{M} = \text{span}(\delta y^i = dy^i + N^i_a(m)dx^a). \tag{2}$$

**Definition 2.3.** *Given a connection $N$ and a solder form $\vartheta$, an associated connection $N-\vartheta$ is defined. Its expression in local coordinates is*

$$N-\vartheta=\left(\frac{\partial}{\partial x^a}-(N_a^i(m)+\vartheta_a^i(m))\frac{\partial}{\partial y^i}\right)\otimes dx^a.$$

If $\mathscr{M}=T\mathscr{B}$, one may be especially interested in the particular case of linear connection meaning that $N_a^i(x,y)=\Gamma_{aj}^i(x)y^j$. In that case, the connection $N-\vartheta_{can}$ will be called the associated linear connection. For a change of the coordinate system on $\mathscr{B}$: $\widetilde{x}^a=\widetilde{x}^a(x^b)$ leading to $\widetilde{y}^i=(\partial\widetilde{x}^i/\partial x^j)y^j$ on $T\mathscr{B}$, the connection coefficient satisfies the specific transformation rule:

$$\frac{\partial\widetilde{x}^b}{\partial x^a}\widetilde{N}_b^k=\frac{\partial\widetilde{x}^k}{\partial x^b}N_a^b-\frac{\partial^2\widetilde{x}^k}{\partial x^a\partial x^b}y^b. \tag{3}$$

For linear connections this implies that $\Gamma$ satisfies the transformation law (64) (properties of the covariant derivative are given in Appendix A.1). This means that from any linear connection $N$ on $\mathscr{M}=T\mathscr{B}$ one obtains a covariant derivative $\nabla$ on $\mathfrak{X}(\mathscr{B})$ with Christoffel symbols $\Gamma$ and vice versa (see [50] for a discussion on covariant derivatives). Remark that all along the paper the terminology *Christoffel symbols* will refer to the coefficient of a covariant derivative or connection (see (63)) and they are not necessarily related to the Riemannian metric.

### 2.3. Parallel and rolling transports

Let $\sigma:[0,1]\to\mathscr{B}; t\mapsto\sigma(t)=(x^a(t))$ be a curve on $\mathscr{B}$. If $\mathscr{B}$ is an open subset of $\mathbb{E}^3$ this curve may be defined by the prescription of its origin $p=\sigma(0)$ and its tangent (velocity) field $\dot{\sigma}(t)=\dot{x}^a(t)\partial/\partial x^a$. For more general (non-Euclidean) manifold $\mathscr{B}$, special attention should be paid to such integration. Indeed, parallel and rolling without slipping transports along $\sigma$ are usually defined for Levi-Civita connection on a Riemannian manifold. In our context, "parallel" refers to the connection $N$ and "rolling" to the connection $N-\vartheta$. The definitions are as follows.

1. Parallel lift of $\dot{\sigma}(t)$ is defined by $\dot{x}^a(\partial/\partial x^a-N_a^i(\sigma(t),y)\partial/\partial y^i)$. Hence, parallel lift of $\sigma$ are obtained by solving
$$\dot{y}^i=-N_a^i(\sigma(t),y)\dot{x}^a.$$

2. Rolling lift of $\dot{\sigma}(t)$ is defined by $\dot{x}^a(\partial/\partial x^a-\left(N_a^i(\sigma(t),y)+\vartheta_a^i(\sigma(t),y)\right)\partial/\partial y^i)$. Hence, rolling lifts of $\sigma$ are obtained by solving
$$\dot{y}^i=-(N_a^i(\sigma(t),y)+\vartheta_a^i(\sigma(t),y))\dot{x}^a.$$

These lifts of the curve starting at any point $(y^i(0))\in\mathscr{M}_{\sigma(0)}$ exist locally and are unique, but may not be well-posed on the whole path $\sigma$ [51–53].

Let us consider the particular case where $\mathscr{M}=T\mathscr{B}$, the connection is linear ($N_a^i(x,y)=\Gamma_{aj}^i(x)y^j$) and the solder form is the canonical one. The coordinate system $(x^a)$ defines a basis $e_i=\delta_i^a\frac{\partial}{\partial x^a}$ in each tangent space. Writing $\mathcal{O}_j^i=\Gamma_{aj}^i(x)dx^a$ and $\mathsf{J}^i=\delta_a^i dx^a$, the above systems can be read as follows.

1. The parallel transport by the connection $N$ of a vector $y^i(0)e_i\in T_p\mathscr{B}$ along $\sigma(t)$ is the vector field $Y(t)=y^i(t)e_i\in T_{\sigma(t)}\mathscr{B}$ obtained by solving the equation
$$\mathrm{d}Y=-\mathcal{O}Y. \tag{4}$$

2. The rolling transport by the connection $N-\vartheta$ of a point $p+y^i(0)e_i\in\mathscr{M}_p$ along $\sigma$ is $\sigma(t)+y^i(t)e_i\in\mathscr{M}_{\sigma(t)}$ where $Y(t)=y^i(t)e_i\in T_{\sigma(t)}\mathscr{B}$ solves the equation
$$\mathrm{d}Y=-\mathcal{O}Y-\mathsf{J}. \tag{5}$$

### 2.4. Curvature and torsion

The total curvature $\mathcal{R}$ of the material (i.e. the bundle $\mathscr{M}$) measures the compatibility of $N-\vartheta$ with Lie brackets of vector fields. For two vector fields $V$ and $W$ on the base manifold $\mathscr{B}$, the curvature,

$$\mathcal{R}(V,W) = (N-\vartheta)\,[V,W] - [(N-\vartheta)V,(N-\vartheta)W]\,,$$

is a vertical vector field on $\mathscr{M}$. This formula can be split into two terms

$$\begin{aligned}\mathcal{R}(V,W) =& \Big(N[V,W] - [NV,NW]\Big)\\ &+ \Big( - [\vartheta V,\vartheta W] + [NV,\vartheta W] + [\vartheta V,NW] - \vartheta[V,W]\Big).\end{aligned}$$

At this step two contributions have to be highlighted.

**Definition 2.4.** *The first term is the Ehresmann curvature, namely $\mathfrak{R}(V,W)$, also called the* curvature of the connection. *The second term is the weak torsion, namely $\mathfrak{T}(V,W)$. We can write $\mathfrak{R} = \mathfrak{R}^i{}_{ab}\dfrac{\partial}{\partial y^i}\otimes dx^a\otimes dx^b$ and $\mathfrak{T} = \mathfrak{T}^i{}_{ab}\dfrac{\partial}{\partial y^i}\otimes dx^a\otimes dx^b$ where their components are respectively given by*

$$\mathfrak{R}^i{}_{ab} = \frac{\partial N^i_b}{\partial x^a} - \frac{\partial N^i_a}{\partial x^b} - N^j_a\frac{\partial N^i_b}{\partial y^j} + N^j_b\frac{\partial N^i_a}{\partial y^j}, \tag{6}$$

$$\mathfrak{T}^i{}_{ab} = -\vartheta^j_a\frac{\partial\vartheta^i_b}{\partial y^j} + \vartheta^j_b\frac{\partial\vartheta^i_a}{\partial y^j} + \frac{\partial\vartheta^i_b}{\partial x^a} - N^j_a\frac{\partial\vartheta^i_b}{\partial y^j} + \vartheta^j_b\frac{\partial N^i_a}{\partial y^j} - \vartheta^j_a\frac{\partial N^i_b}{\partial y^j} - \frac{\partial\vartheta^i_a}{\partial x^b} + N^j_b\frac{\partial\vartheta^i_a}{\partial y^j}. \tag{7}$$

The geometrical interpretation of the curvature is as follows.

**Lemma 2.5.** *If the curvature of a connection vanishes, then the lift of any loop $\sigma$ on base manifold $\mathscr{B}$, when defined, is closed [52, 53].*

One obtains two connections from one, adding or not the solder form. In general, the vanishing of $\mathcal{R}$ and the vanishing of $\mathfrak{R}$ are independent. When the connections have a special structure, it can happen that $\mathcal{R}$ controls $\mathfrak{R}$ as is the case in the linear situation below where $\mathcal{R}=0$ implies $\mathfrak{R}=0$ and $\mathfrak{T}=0$.

**Lemma 2.6.** *Let us consider the case where $\mathscr{M} = T\mathscr{B}$ and $N$ is linear, meaning that $N^i_a(x,y) = \Gamma^i_{aj}(x)y^j$, and $\vartheta = \vartheta_{can}$. It follows by direct computation:*

$$\mathfrak{R}^i{}_{ab} = \Big(\frac{\partial\Gamma^i_{bj}}{\partial x^a} - \frac{\partial\Gamma^i_{aj}}{\partial x^b} + \Gamma^k_{bj}\Gamma^i_{ak} - \Gamma^k_{aj}\Gamma^i_{bk}\Big)y^j = \mathsf{R}^i_{jab}y^j, \tag{8}$$

$$\mathfrak{T}^i{}_{ab} = \vartheta^j_b\Gamma^i_{aj} - \vartheta^j_a\Gamma^i_{bj} = \mathsf{T}^i{}_{ab}. \tag{9}$$

*Here $\mathsf{R}$ and $\mathsf{T}$ are respectively the associated curvature and torsion tensor of the covariant derivative $\nabla$ associated with Christoffel symbols $\Gamma$ (see Appendix A.1). In this sense the derived tensors $\mathfrak{R}$ and $\mathfrak{T}$ of the connection $N$ on $\mathscr{M}$ are a geometrical reformulation of the ones of $\nabla$ on $\mathfrak{X}(\mathscr{B})$.*

The curvature and torsion can be interpreted as an obstruction: recall that the rolling transport of $Y=(y^i)\in\mathscr{M}_p$ along the path $\sigma$ is obtained by solving the Equations (5): $\mathrm{d}Y = -\mathcal{O}Y - \mathsf{J}$. Solutions may depend on the chosen path. It is not always possible to solve this system. In practice, this is possible if and only if $\mathrm{d}\mathrm{d}Y = 0$, otherwise the multivaluedness of the problem is characterised by the non-vanishing of

$$\mathrm{d}\mathrm{d}Y = -(\mathrm{d}\mathcal{O} + \mathcal{O}\wedge\mathcal{O})Y - (\mathrm{d}\mathsf{J} + \mathcal{O}\wedge\mathsf{J}). \tag{10}$$

The first component $\mathrm{d}\mathcal{O}+\mathcal{O}\wedge\mathcal{O}$ is the usual curvature matrix valued two-form $\mathsf{R}$. The second term $\mathrm{d}\mathsf{J}+\mathcal{O}\wedge\mathsf{J}$ is the torsion vector valued two-form of $\mathsf{T}$. Both are tensors over $\mathscr{B}$. The total curvature vanishes if and only if both the usual curvature and the usual torsion vanish.

### 2.5. Sasaki metric

At this stage, no metric tensor g has to be prescribed on $\mathscr{M}$. This latter is then, at this stage, a free parameter that could complete the characterisation of the material manifold. In the following, particular metrics would appear naturally. These are Sasaki metrics [54–56] defined by

$$\mathfrak{g}(m) = \mathrm{g}^{h}_{ab}(m)dx^a \otimes dx^b + \mathrm{g}^{v}_{ij}(m)\delta y^i \otimes \delta y^j. \tag{11}$$

The first term is called the horizontal metric and the other is the vertical metric.

The benefit of this type of metric is that the split structure of the metric is preserved under any change of coordinates. This effect is ensured by the proper bases of such metric tensor that preserve the split structure of the tangent space $T\mathscr{M}$ involved by using the Ehresmann connection $N$. Indeed, it was stressed in (1) and (2) that for a given Ehresmann connection, the non-holonomic bases $(\delta_a, \partial_i)$ and $(dx^a, \delta y^i)$ are convenient local bases on $T\mathscr{M}$ and $T^*\mathscr{M}$, respectively. In practice, this illustrates that the notion of angle and length are meaningful only if such quantities are related to neighbouring points belonging to the same micro- or macro-universe. More precisely, the horizontal metric is related to the macroscopic observations on the material, whereas the vertical part is related to points belonging to a given microelement.

### 2.6. Toward transformation of microstructured media

On the one hand, a continuum with microstructure is assumed to be a tangent bundle over a three-dimensional differentiable manifold $\mathscr{B}$. On the other hand, $\mathbb{E}^3$ is the three-dimensional Euclidean space. For instance, a fibre morphism or so-called bundle map $\mathscr{M} \to T\mathbb{E}^3$ presents the evolution of the microstructured material manifold $\mathscr{M}$ in the Euclidean space [52, 53]. It may possibly depend on time. By a language shortcut, such a bundle map is sometimes called transformation hereafter.

The configuration of the body is described by the geometrical structure induced by the pull-back from $T\mathbb{E}^3$ onto $\mathscr{M}$. This current-induced geometry must be able to reveal if material defects are present or created by a material transformation. The main objective of this paper is to specify how such a defective configuration is obtained via such a type of bundle mapping or generalisation of this latter.

In particular, the complete characterisation of the current configuration needs to specify how measures and variations are performed around an infinitesimal neighbourhood of an element of $\mathscr{M}$. Such information is encoded on the covariant derivative $\nabla$ and the metric tensor. These tensors are acting on elements on $T\mathscr{M}$. In other words, the full configuration is controlled by the bundle map $T\mathscr{M} \to TT\mathbb{E}^3$. The following section is dedicated to this crucial point.

## 3. Scaled material model

Here a special model is presented. It is restricted to the particular case where $\mathscr{M}$ is isomorphic to $T\mathscr{B}$ and where the solder form is canonical (in the following $\vartheta = \vartheta_{can}$).

Let us first recall some standard conventions. We use $(X^A, Y^I)$ (respectively, $(x^a, y^i)$) to denote a chart on $\mathscr{M}$ (respectively, $T\mathbb{E}^3$). The Euclidean space $\mathbb{E}^3$ has a canonical affine connection, namely the Levi-Civita connection $\gamma$ of the Euclidean metric g (of course, if Cartesian chart is used on the Euclidean space, the connection coefficients vanish). Its tangent bundle, as any tangent bundle, has a canonical solder form denoted by $\underline{\delta}$ as its components $(\delta^i_a)$ in any frame of $\mathbb{E}^3$ coincide with those of the identity. Finally, the tangent bundle of the Euclidean space may be equipped with a trivial Ehresmann connection (with coefficients $n^i_a(x,y) = \gamma^i_{aj}(x)y^j$ in a local coordinate system) and with a metric tensor $\mathfrak{g}$ having a Sasaki form:

$$\mathfrak{g} = \mathrm{g}_{ab}(x)dx^a \otimes dx^b + \mathrm{g}_{ij}(x)\delta y^i \otimes \delta y^j. \tag{12}$$

Define $(E^K) = (dX^A, dY^I)$ with $K$ running from 1 to 6, the first three basis elements are $dX^A$, the others are $dY^I$ ($A$ and $I$ run from 1 to 3). Similarly, $(e_k) = (\partial_a, \partial_i)$ with $k$ running from 1 to 6. The first three basis elements denote the $\partial_a$ basis, the others coincide with $\partial_i$.

A geometrical transformation $\phi : \mathscr{B} \to \mathbb{E}^3$ is inducing an "idealised" material transformation $\mathscr{M} \to T\mathbb{E}^3$ using the derivative and the canonical solder form : $(X, Y) \mapsto (\phi(X), \underline{\delta}F(X)\vartheta(Y))$ with $F = \phi_*$. In local coordinates the latter can be written: $\delta^i_a F^a_A \vartheta^A_I Y^I$. From now on, the formula will be shortened as $F^i_I Y^I$. In that way, we define $F^i_I = \delta^i_a F^a_A \vartheta^A_I$ and $F^a_I$ denotes $F^a_A \vartheta^A_I$.

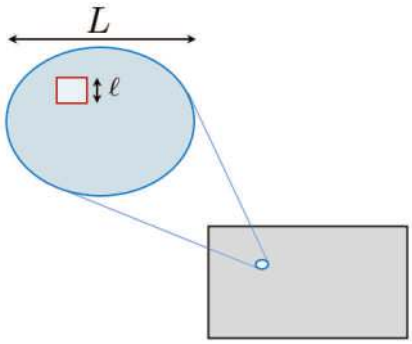


**Figure 2.** Various length scales of a model: microscopic and macroscopic. The scale ratio $\ell/L$ is defined to account for scaling effects.

### *3.1. Overall approach*

In most of standard works on the geometrical analysis of defective media, the tangent transformation $T\mathscr{M} \to TT\mathbb{E}^3$ is induced by the derivative of $\mathscr{M} \to T\mathbb{E}^3$ but this choice is not a strict constraint and could be relaxed. For this purpose, an Ehresmann connection has to be created. In the present paper, the solder form defined on $T\mathscr{B}$ is always assumed to be the canonical form. The Ehresmann connection may be linear or not. However, in the following, special attention is given to the linear case for which Ehresmann curvature and weak torsion will coincide with those defined through covariant derivatives, see Section 2.4.

It is assumed that the continuum consists of a huge number of infinitesimal volume elements $dV$, located at a mathematical point $p$ in the base manifold $\mathscr{B}$ ($p$ may be interpreted as the centre of mass of $dV$, see Figure 2). The motion of $p$ is governed by the map $\phi$. Deformation of $dV$ is controlled by $F = \phi_*$. In addition, the volume elements $dV$ are composed of a large number of sub-domains/microelements $\delta V$ of finite (but tiny) size. As $\delta V$ contains a finite quantity of matter, its stretch may be considered. In this context, the continuum is deformed by two independent maps: $F$ defines the stretch at a macroscopic scale, whereas $\Theta$ defines the stretch at a microscopical scale.

If the material transformation is described by the bundle mapping $\mathscr{M} \to T\mathbb{E}^3, (X, Y) \mapsto (\phi(X), \Theta(X)Y)$ the scaling effect is not easily tractable as $F$ and $\Theta$ are acting on a vector belonging to $T_p\mathscr{B}$ and $\mathscr{M}_p$, respectively, that are equivalent manifolds (as $\mathscr{M} = T\mathscr{B}$, then $\mathscr{M}_p = T_p\mathscr{B}$). This difficulty can be circumvented in the following way: let us consider that the local change of a vector $Y$ associated with the microstructure and belonging to $\mathscr{M}$, is measured by an element $Z^v$ of $V(\mathscr{M})$. Hence, the material transformation is represented by a smooth map

$$\Upsilon^v : V(\mathscr{M}) \to VT\mathbb{E}^3, \quad (X, Y, Z^v) \mapsto (\phi(X), \underline{\delta}F(X)\vartheta\, Y, \Theta(X)Z^v), \tag{13}$$

where $\Theta(X)$ is smooth, invertible and orientation preserving. Accordingly, such sub-scale modelling is no longer redundant because the maps related to each scale are separated.

To construct an induced Ehresmann connection the first idea is to extend $\Upsilon^v$ to the whole space, i.e. find a bundle map $\Upsilon$: $T\mathscr{M} \to TT\mathbb{E}^3$ of the form

$$(X, Y, Z) \mapsto (\phi(X), \underline{\delta}F(X)\vartheta\, Y, \Omega(X, Y)Z),$$

with $X \in \mathscr{B}$, $Y \in \mathscr{M}_X$ and $Z \in T_{(X,Y)}\mathscr{M}$. At this stage, attention is now focused on $\Omega = \Omega^k_K e_k \otimes E^K$ or, in detail,

$$\Omega = \Omega^a_A \partial_a \otimes dX^A + \Omega^a_I \partial_a \otimes dY^I + \Omega^i_A \partial_i \otimes dX^A + \Omega^i_I \partial_i \otimes dY^I,$$

for which one has a great freedom of choice. The image of $(X, Y)$ is already partially prescribed. Indeed, as the restriction of $\Upsilon$ for any element of $V(\mathscr{M})$ is imposed by (13):

$$\Omega^i_I(X, Y) = \Theta^i_I(X).$$

In order to avoid too complex interpretations, a second idea is proposed by considering that if $\Theta = F$ the scaling effect must not be observed. Then, if $\Theta = F$, the material transformation has to coincide with the simpler one $\mathcal{H} : \mathscr{M} \to T\mathbb{E}^3, (X, Y) \mapsto (\phi(X), \underline{\delta}F(X)\vartheta\, Y)$ for which $\Omega$ is nothing else than the total gradient $\mathcal{H}_*$. Accordingly, one obtains

$$\Omega^a_A(X, Y) = F^a_A(X) \qquad \text{and} \qquad \Omega^a_I = 0.$$

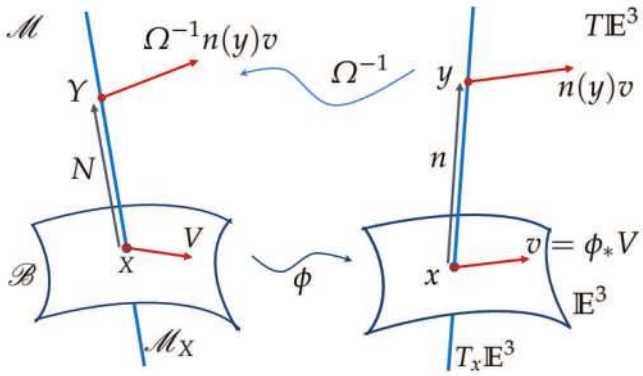


**Figure 3.** Pictorial representation of an induced Ehresmann connection.

### 3.2. *Induced structure*

At this stage $\Omega$ takes the following form:

$$\Omega = F^a_A \partial_a \otimes dX^A + \Omega^i_A \partial_i \otimes dX^A + \Theta^i_I \partial_i \otimes dY^I, \tag{14}$$

where the choice of $\Omega^i_A(X, Y)$ is still free. The inverse of $\Omega$ is given by $\Omega^{-1} = \Omega^K_k E_K \otimes e^k$ with $\Omega^K_k \Omega^\ell_K = \delta^\ell_k$ and $\Omega^K_k \Omega^k_L = \delta^K_L$. This latter is of the form:

$$\Omega^{-1} = F^A_a \partial_A \otimes dx^a + \Omega^I_a \partial_I \otimes dx^a + \Theta^I_i \partial_I \otimes dy^i, \tag{15}$$

where $\Theta^I_i \Theta^j_I = \delta^j_i$ and $F^A_a F^b_A = \delta^b_a$.

Let $V$ be an arbitrary tangent vector to $\mathscr{B}$ at a point $X \in \mathscr{B}$, the induced Ehresmann connection is naturally defined by considering its horizontal lift given by (a pictorial interpretation is given in Figure 3)

$$\begin{aligned} N(X, Y)V &= \Omega^{-1}\Big(n(\phi(X), \underline{\delta} F(X)\vartheta Y)(\phi_* V)\Big) \\ \text{with coefficients} \quad N^I_A &= \Theta^I_i \Omega^i_A + \Theta^I_i n^i_a F^a_A. \end{aligned} \tag{16}$$

Here, we recall that $n$ is the ambient Ehresmann connection with the connection coefficients are $n^i_a(x, y) = \gamma^i{}_{aj}(x) y^j$, and $\gamma$ is the Levi-Civita connection given on $\mathbb{E}^3$ (see the beginning of Section 3). The proof of (16) is detailed in Appendix A.2. Note that the definition of the induced connection is independent on the chosen chart.

**Proposition 3.1.** *If the manifold $\mathscr{M}$ is endowed with the connection $N$ given in* (16)*, one obtains*

$$\Omega = F^a_A \frac{\delta}{\delta x^a} \otimes dX^A + \Theta^i_I \frac{\partial}{\partial y^i} \otimes \delta Y^I. \tag{17}$$

Hence, $\Omega$ may be seen as the collection of two maps: $H_m(\mathscr{M}) \to H_{(x,y)} T\mathbb{E}^3$ and $V_m(\mathscr{M}) \to V_{(x,y)} T\mathbb{E}^3$. Roughly speaking, this states the existence of two independent mechanisms, the first is the ordinary dragging of vectors by means of the deformation gradient $F = \phi_*$ of the macrostructure; the second is associated with the transformation $\Theta$ of the microstructure.

**Proof.** Without loss of generality, the Cartesian coordinate system is used on $T\mathbb{E}^3$ and accordingly $\delta/\delta x^a = \partial_a$. Considering that $\Omega^i_I \Omega^I_j = \Theta^i_I \Omega^I_j = \delta^i_j$, one obtains

$$\Omega = F^a_A \frac{\delta}{\delta x^a} \otimes dX^A + \Theta^i_I \frac{\partial}{\partial y^i} \otimes (\Omega^I_j \Omega^j_A \, dX^A + dY^I).$$

The proof ends because $N^I_A = \Omega^I_i \Omega^i_A$ and $\delta Y^I = N^I_A dX^A + dY^I$. □

Usually, the induced metric is given by $\mathcal{G} = \Omega^* \mathfrak{g}$ or explicitly $\mathcal{G}(V,U) = \mathfrak{g}(\Omega V, \Omega U)$ for all $V, U \in T\mathscr{M}$. According to the connection $N$ given in (16), metric tensor $\mathcal{G}$ has a Sasaki structure:

$$\begin{aligned} \mathcal{G}(X,Y) = {} & \mathtt{G}^h{}_{AB}(X) dX^A \otimes dX^B + \mathtt{G}^v{}_{IJ}(X) \delta Y^I \otimes \delta Y^J \\ \text{with} \quad & \mathtt{G}^h{}_{AB} = F^a_A \mathfrak{g}_{ab} F^b_B, \qquad \mathtt{G}^v{}_{IJ} = \Theta^i_I \mathfrak{g}_{ij} \Theta^j_J. \end{aligned} \tag{18}$$

Their components are just functions of the base coordinate $X$: the metric is uniquely defined at a given point $p$ of $\mathscr{B}$. In addition, it can be seen that the vertical metric component is always given by $\mathtt{G}^v{}_{IJ} = \mathcal{G}(\partial_I, \partial_J) = \Theta^i_I \mathfrak{g}_{ij} \Theta^j_J$ what is explicitly independent on the definition of the Ehresmann connection $N$ (even if this letter is a key ingredient of the definition of proper bases of horizontal and vertical space, see (1) and (2)). More precisely, the components of $\mathcal{G}$ in the proper horizontal and vertical bases are completely specified by $\Upsilon^v$ and they are independent of the choice of the (possibly non-linear) connection $N(X,Y)$.

From (17) and (18) it is observed that microscopic and macroscopic processes are naturally separated. More specifically, for the microscopic process, the solder form is an important tool that relates the microscopic quantities (belonging to $V(\mathscr{M})$) to macroscopic quantities (belonging to $T\mathscr{B}$). By way of illustration, let us consider a vector field $V = V^A \partial/\partial X^A$ on $\mathscr{B}$. Its canonical vertical lift is $\vartheta V = \delta^I_A V^A \partial/\partial Y^I$ at any point along the fibre $T_X\mathscr{B}$. The vertical metric $\mathtt{G}^v$ induces a metric $\mathtt{G}$ on $\mathscr{B}$ defined by $\mathtt{G}(X)(V,W) = \mathtt{G}^v(X)(\vartheta V, \vartheta W)$ for every $V, W \in T_X\mathscr{B}$. In a coordinates system:

$$\mathtt{G}_{AB} = \vartheta^I_A \Theta^i_I \mathfrak{g}_{ij} \Theta^j_J \vartheta^J_B \qquad \Big(\text{in short} \quad \mathtt{G}_{AB} = \Theta^a_A \mathfrak{g}_{ab} \Theta^b_B\Big). \tag{19}$$

This metric $\mathtt{G}$ may be chosen as a measure on $\mathscr{B}$ of the current configuration of the microstructure. The construction of the connection $N$ from this split structure allows us to interpret macroscopically a change of microscopic quantities, this is evident through the mixed indices of the connection $N^I_A$.

### 3.3. Linear induced connection

Recall that the Euclidean space $\mathbb{E}^3$ has a canonical connection: the Levi-Civita connection $\gamma$ of the Euclidean metric g. More precisely, the trivial Ehresmann connection $n$ has the form $n^i_a(x,y) = \gamma^i_{aj} y^j$.

**Lemma 3.2.** *The connection is linear, i.e. $N^I_A(X,Y) = \Gamma^I_{AJ}(X) Y^J$ if and only if $\Omega^i_A(X,Y)$ is linear that means $\Omega^i_A(X,Y) = \Omega^i_{AJ}(X) Y^J$. In that case, one obtains*

$$\Gamma^I_{AJ} = \Theta^I_i \Omega^i_{AJ} + \Theta^I_i \gamma^i_{aj} F^j_J F^a_A, \tag{20}$$

*and if Cartesian coordinates are applied on $T\mathbb{E}^3$, $\Gamma^I_{AJ} = \Theta^I_i \Omega^i_{AJ}$; where the following notation are recalled, $F^a_I = F^a_A \vartheta^A_I$ and $F^j_I = \delta^i_a F^a_A \vartheta^A_I$.*

**Proof.** It is directly thanks to (16) as $\Theta$ is independent of $Y$. Keep in mind that $n^i_a = \gamma^i_{aj}(x) y^j$ with $x = \phi(X)$ and $y = \underline{\delta} F \vartheta Y$, then straightforward computations give $N^I_A(X,Y) = \Theta^I_i \Omega^i_A - \Theta^I_i n^i_a F^a_A = \Theta^I_i \Omega^i_{AJ} Y^J - \Theta^I_i \gamma^i_{aj} y^j F^a_A = \Theta^I_i \Omega^i_{AJ} Y^J - \Theta^I_i \gamma^i_{aj} F^j_J Y^J F^a_A$ which verifies (20). □

One considers hereafter $\Omega^i_A(X,Y) = \Omega^i_{AI}(X) Y^I$ where $\Omega^i_{AI}$ is free up to now. In order to remove this indeterminacy, $\Omega^i_{AI}$ is constructed by a linear balance between the stretching variations at each scale (Figure 2):

$$\boxed{\Omega^i_{AI} = (1-\zeta) \partial_A F^i_I + \zeta \partial_A \Theta^i_I,} \tag{21}$$

where $0 < \zeta \leq 1$ is a free parameter controlling the scaling effect. For example, and without any loss of generality, it can be defined as $\zeta = \ell/L$ where $L$ and $\ell$ are the macroscopic and microscopic characteristic scales, respectively. The parameter $\zeta$ is called the *scaling factor* hereafter.

The map $\Omega$ coincides with the total gradient of a linear bundle map $\mathscr{M} \to T\mathbb{E}^3, (X,Y) \mapsto (\phi(X), \underline{\delta} F(X) \vartheta Y)$ if $\Theta^i_I = F^i_I$. On the other hand, if $\zeta = 1$, the transformation coincides formally with the total gradient of $\mathscr{M} \to T\mathbb{E}^3, (X,Y) \mapsto (\phi(X), \Psi(X) Y)$ with $\Psi^i_I = \Theta^i_I$ (note that $\Psi$ and $\Theta$ are not exactly the same tensor as they act on different spaces: $\mathscr{M}_p$ and $V_m(\mathscr{M})$, respectively).

**Corollary 3.2.1.** *If $\Omega^i_A$ satisfies* (21)*, then one obtains*

$$\Gamma^I_{AJ} = \Theta^I_i\big((1-\zeta)\partial_A F^i_I + \zeta\partial_A\Theta^i_I\big) + \Theta^I_i\gamma^i_{aj}F^j_J F^a_A, \tag{22}$$

*and if a Cartesian chart applied on $T\mathbb{E}^3$ is used, $\gamma^i_{aj} = 0$ gives*

$$\boxed{\Gamma^I_{AJ} = \Theta^I_i\big((1-\zeta)\partial_A F^i_J + \zeta\partial_A\Theta^i_J\big).} \tag{23}$$

### *3.4. Induced torsion, curvature and non-metricity tensor*

As the induced Ehresmann connection $N$ is linear and the solder form defined on the tangent bundle is the canonical form, the affine connection $\Gamma$ and the connection $N$ contain the same information. Hence, the following results are presented with $\Gamma$ instead of $N$. From these connections and metric, it is easy to obtain the driven geometrical quantities such as curvature, torsion and non-metricity tensors.

First, the torsion of the connection is given by

$$\begin{aligned}
\mathsf{T}^I{}_{AB} &= \vartheta^J_B\Gamma^I_{AJ} - \vartheta^J_A\Gamma^I_{BJ},\\
&= (1-\zeta)\Theta^I_i\left(\delta^J_B\partial_A F^i_J - \delta^J_A\partial_B F^i_J\right) + \zeta\Theta^I_i\left(\delta^J_B\partial_A\Theta^i_J - \delta^J_A\partial_B\Theta^i_J\right),\\
&= (1-\zeta)\Theta^I_i\delta^i_c\left(\partial_A F^c_B - \partial_B F^c_A\right) + \zeta\Theta^I_i\left(\delta^J_B\partial_A\Theta^i_J - \delta^J_A\partial_B\Theta^i_J\right),\\
&= \zeta\Theta^I_i\left(\delta^J_B\partial_A\Theta^i_J - \delta^J_A\partial_B\Theta^i_J\right).
\end{aligned} \tag{24}$$

Here, we have used the fact that, because $F = \phi_*$, then $\partial_A F^c_B = \partial_B F^c_A$. The torsion is proportional to the scaling factor $\zeta$. Second, the induced curvature of the connection is directly obtained from (8):

$$\mathsf{R}^I_{JAB} = \Omega^i_{BJ}\partial_A\Theta^I_i - \Omega^i_{AJ}\partial_B\Theta^I_i + \Theta^I_i\Theta^K_j\Big(\Omega^i_{BJ}\Omega^j_{AK} - \Omega^i_{AJ}\Omega^j_{BK}\Big). \tag{25}$$

According to (21) the curvature contains both linear and quadratic dependency on the scaling factor. Finally, the connection may be not compatible with the vertical metric. This is measured by the non-metricity tensor $\mathsf{Q} = \nabla\mathsf{G}$ for which components are $\mathsf{Q}_{IJA} = \nabla_A\mathsf{G}_{IJ}$. The general formulae for these coefficients are given in Appendix A.2. For Cartesian coordinates on the Euclidean space, $\mathrm{g}_{ij} = \delta_{ij}$ and the Christoffel symbols are $\gamma^k_{ij} = 0$, in such a case the formulae are simpler:

$$\begin{aligned}
\mathsf{Q}_{IJA} &= \partial_A\mathsf{G}_{IJ} - \Gamma^K_{AI}\mathsf{G}_{KJ} - \Gamma^K_{AJ}\mathsf{G}_{IK},\\
&= (1-\zeta)\left(\Theta^i_J\partial_A\big(\Theta^i_I - F^i_I\big) + \Theta^i_I\partial_A\big(\Theta^i_J - F^i_J\big)\right).
\end{aligned} \tag{26}$$

The metric is compatible with the connection, i.e. $\mathsf{Q} = 0$ if $\zeta = 1$ (no scaling effect) or if $\Theta = F$ (Euclidean manifold). The condition for metricity of the connection can be written as (in Cartesian coordinates on $\mathbb{E}^3$)

$$\Theta^i_J\partial_A\big(\Theta^i_I - F^i_I\big) = -\Theta^i_I\partial_A\big(\Theta^i_J - F^i_J\big), \quad \forall\, I,J,A, \tag{27}$$

meaning that, for any $A$, the tensor $\Theta^i_I\partial_A\big(\Theta^i_J - F^i_J\big)\partial_I\otimes\partial_J$ must be skew symmetric.

### *3.5. Synthesis*

The manifold $(\mathscr{M},\Gamma,\mathcal{G})$ provides a complete description of the current configuration of the microstructured material. If (21) is assumed, it is governed by three independent quantities $\phi,\Theta$ and $\zeta$. The split structure of the transformation and metrics, underlined at the end of Section 3.2, allows us to describe the current state as the superposition of a microscopic and macroscopic processes. These latter processes are coupled as they are driven by the same kinematical quantities $\phi$ and $\Theta$. The scalar $\zeta$ governs such coupling, this has motivated the *scaling factor* name. The structure of the problems enables us to describe the current configuration on $\mathscr{B}$ by defining a micro-manifold $(\mathscr{B},\Gamma,\mathsf{G})$ with $\mathsf{G}\equiv\mathsf{G}^v$ (see (19)) and a macro-manifold $(\mathscr{B},\mathsf{L},\mathsf{G}^h)$ with

$$\mathsf{L}^C_{AB} = \frac{1}{2}\mathsf{G}^{hCD}\big(\partial_A\mathsf{G}^h{}_{BD} + \partial_B\mathsf{G}^h{}_{AD} - \partial_D\mathsf{G}^h{}_{AB}\big), \tag{28}$$

being the Christoffel symbols of the horizontal metric. This connection has no torsion and no curvature and is metric compatible. The properties of $(\mathscr{B}, \Gamma, \mathsf{G})$ are richer.

**Proposition 3.3.** *If $\Omega^i_A$ satisfies Lemma 3.2, with $\Omega^i_{AJ}$ satisfying* (21)*, the manifold $(\mathscr{B}, \Gamma, \mathsf{G})$ has the following properties.*

*•If $\Theta = F$, then macro and micro elements behave in the same way. It yields that $\mathsf{T} = 0$; $\mathsf{R} = 0$ and $\nabla \mathsf{G} = 0$. The manifold behaves as an Euclidean space.*
*•If $\zeta = 1$, then the scaling effect is no longer considered. In that case, the manifold behaves as a Weitzenböck manifold with $\mathsf{T} \neq 0$, $\mathsf{R} = 0$ and $\nabla \mathsf{G} = 0$.*
*•If $\zeta \to 0$, then the size of the microstructure tends to be negligible. Even if $\mathsf{T} \to 0$, one may observe $\mathsf{R} \neq 0$ and $\nabla \mathsf{G} \neq 0$. In particular, if $\nabla \mathsf{G} = 0$ the manifold tends to behave as a RC manifold.*
*•If $\Theta \neq F$ and $0 < \zeta < 1$, then $\mathsf{T} \neq 0$, $\mathsf{R} \neq 0$ and $\nabla \mathsf{G} \neq 0$. The manifold behaves as a Weyl manifold.*

## 4. Alternative approaches

### 4.1. Non-scale material modelling

In the previous section, the material transformation has been enriched by introducing a map $\Theta$ specifying how the vector belonging to $V(\mathscr{M})$ is transformed independently on $\phi$. An alternative method consists of prescribing an enrichment on the tangent map acting on $\mathscr{M}_p = T_p\mathscr{B}$. In such a case, the transformation is specified by the bundle map:

$$\mathcal{H} \,:\, \mathscr{M} \to T\mathbb{E}^3, \quad (X, Y) \mapsto (\phi(X), \Psi(X, Y)), \tag{29}$$

where $\Psi(X, Y)$ is supposed to be smooth, with a smooth inverse and satisfies the condition that $\Psi(X, Y) = 0$ if and only if $Y = 0$. Accordingly, the total gradient $\mathcal{H}_* = D\mathcal{H}$ of the bundle mapping is given by

$$\begin{aligned} \mathcal{H}_* &= \mathcal{H}^k_K \, e_k \otimes E^K = \partial_K \mathcal{H}^k \, e_k \otimes E^K, \\ &= \partial_A \phi^a \, \partial_a \otimes dX^A + \partial_A \Psi^i \, \partial_i \otimes dX^A + \partial_I \Psi^i \, \partial_i \otimes dY^I. \end{aligned} \tag{30}$$

Its inverse is given by $\mathcal{H}^* = \mathcal{H}^K_k E_K \otimes e^k$ with $\mathcal{H}^K_k \mathcal{H}^\ell_K = \delta^\ell_k$ and $\mathcal{H}^K_k \mathcal{H}^k_L = \delta^K_L$. It gives explicitly:

$$\mathcal{H}^* = F^A_a \partial_A \otimes dx^a + \partial_a \Psi^I \partial_I \otimes dx^a + \partial_i \Psi^I \partial_I \otimes dy^i. \tag{31}$$

With the same spirit as (16), an induced Ehresmann connection is obtained by

$$\begin{aligned} N(Y)V &= \mathcal{H}^* \Big( n\big(\phi(X), \Psi(X, Y)\big) \phi_* V \Big) \\ \text{with coefficients} \qquad N^I_A &= \partial_j \Psi^I n^j_a F^a_A + \partial_i \Psi^I \partial_A \Psi^i. \end{aligned} \tag{32}$$

The proof is given in Appendix A.2. The induced connection is not necessarily linear as soon as it is not the case for $\Psi(X, Y)$.

**Lemma 4.1.** *The associated Ehresmann curvature $\mathfrak{R}$ always vanishes.*

**Proof.** From Definition 2.4, for arbitrary vector fields $V$ and $U$ on $\mathscr{B}$, one has

$$\begin{aligned} \mathfrak{R}(V, U) &= N\,[V, U] - [NV, NU] \\ &= \mathcal{H}^* \big( n\,(\phi_*\,[V, U]) \big) - \big[ \mathcal{H}^*(n\,(\phi_* V)), \mathcal{H}^*(n\,(\phi_* U)) \big] \\ &= \mathcal{H}^* \big( n\,([\phi_* V, \phi_* U]) \big) - \mathcal{H}^*\,[n\,(\phi_* V)\,, n\,(\phi_* U)]\,. \end{aligned}$$

As the curvature of the connection $n$ vanishes, $n([\phi_* V, \phi_* U]) = [n(\phi_* V), n(\phi_* U)]$. This implies $\mathfrak{R}(U, V) = 0$ yielding that the Ehresmann curvature $\mathfrak{R}$ vanishes.[1] □

To go further the pull-back operator has not to be defined by the total gradient $\mathcal{H}_*$. This is exactly what has been done in the *scaled material model sec*-3.

**Proposition 4.2.** *If the manifold $\mathscr{M}$ is endowed with the connection $N$, the total gradient $\mathcal{H}_*$ becomes*

$$\mathcal{H}_* = F^a_A \frac{\delta}{\delta x^a} \otimes dX^A + \partial_I \Psi^i \frac{\partial}{\partial y^i} \otimes \delta Y^I. \tag{33}$$

Next, an induced metric is defined by $\mathcal{G} = \mathcal{H}^* \mathfrak{g}$, i.e. $\mathcal{G}(V, U) = \mathfrak{g}(\mathcal{H}_* V, \mathcal{H}_* U)$ with $V, U \in T\mathscr{M}$. With respect to the connection $N$, this tensor splits like a Sasaki metric:

$$\begin{aligned} \mathcal{G}(X, Y) = {} & \mathbb{G}^h{}_{AB}(X) dX^A \otimes dX^B + \mathbb{G}^v{}_{IJ}(X, Y) \delta Y^I \otimes \delta Y^J, \\ \text{with} \quad & \mathbb{G}^h_{AB} = F^a_A \mathfrak{g}_{ab} F^b_B, \qquad \mathbb{G}^v_{IJ} = \partial_I \Psi^i \mathfrak{g}_{ij} \partial_J \Psi^j. \end{aligned} \tag{34}$$

Similarly, it can be seen that the vertical metric components are always given by $\mathbb{G}^v{}_{IJ} = \mathcal{G}(\partial_I, \partial_J) = \partial_I \Psi^i \mathfrak{g}_{ij} \partial_J \Psi^j$, then the vertical metric is independent on the induced connection $N$.

Keeping in mind that our objective was to construct a linear Ehresmann connection with torsion and curvature, the present bundle maps fails for the following reasons: (1) the vertical metric $\mathbb{G}^v(X, Y)$ is generally dependent on fibre coordinate; (2) the connection is not linear; (3) the curvature of the connection is always zero.

However, in the linear situation for which $\Psi^i(X, Y) = \Psi^i_I(X) Y^I$, the non-scale material modelling may be seen as a subset of the scaled material model. Indeed, the micro-manifold on $\mathscr{B}$ (specified in Section 3.5) shares the same properties as the manifold induced by (29) if $\Theta = \Psi$ and/or $\zeta = 1$. More precisely, one obtains the following result.

**Theorem 4.3.** *If* (29) *is linear, one obtains:*

- $N^I_A(X, Y) = \Gamma^I_{AJ}(X) Y^J$; with $\Gamma^C_{AB} = \Psi^C_c \partial_A \Psi^c_B$ *if Cartesian coordinates are used on* $T\mathbb{E}^3$;
- *the metric* $\mathbb{G}^v$ *induces a metric on* $\mathscr{B}$ *by* $\mathbb{G} = \vartheta^* \mathbb{G}^v$, *locally* $\mathbb{G}_{AB} = \Psi^a_A \mathfrak{g}_{ab} \Psi^b_B$.

*This elements construct a Weitzenböck manifold* $(\mathscr{B}, \Gamma, \mathbb{G})$ *with metric-compatible connection and torsion with vanishing curvature. Obviously, if* $\Psi = F$ *no defect appears meaning that the torsion and curvature of the connection vanish.*

**Remark 4.4.** *It must be noted that the presented approach may be interestingly compared with continuum modelling using (pseudo-)Finsler geometry. In a Finsler space the connection and its driven geometric quantities (curvature, etc.) are generated by a metric tensor that is defined by a fundamental scalar function* $L(X, Y)$. *This is defined at every point (except for* $Y = 0$*) and is homogeneous of degree one in* $Y$ *[54, 57]. Such geometrical construction affords a great generality for describing several phenomena in physics. Application of (pseudo-)Finsler geometry in continuum mechanics and physics have been suggested earlier by [58], later by [59–61], and recently by [56, 62–65]. Non-conservative mechanical systems may be explored through a non-linear connection in the Riemannian and Finslerian framework [66]. Such non-linear connections are mainly used to express the non-linear relation between fields having different natures [67].*

### 4.2. Comparison with the non-holonomic principle

The forms of the metric and the connection presented in Theorem 4.3 looks qualitatively similar to those in numerous other defect-theories [10, 12, 14, 20, 68]. Among them, one of the most powerful tools is the *non-holonomic principle* [13, 21, 23]. In this context, the continuum is modelled by a differential manifold $\mathscr{B}$ supporting a non-standard material transformation: a map from $\mathscr{B}$ into $\mathbb{E}^3$, $X \mapsto x$, which is not smooth in general and may be multivalued (to simplify problem we assume $(x^a)$ to be a Cartesian coordinates system). However, it is possible to map the points surrounding $X$ defined by the tangent vector $dX$ to $dx$ via an infinitesimal transformation thanks to tetrads $\mathbf{e}^a_A$ such that

$$dx^a = \mathbf{e}^a_A dX^A. \tag{35}$$

Their reciprocal tetrads are introduced by $\mathbf{e}^a_A \mathbf{e}^A_b = \delta^a_b$ and $\mathbf{e}^a_A \mathbf{e}^B_a = \delta^B_A$.

**Remark 4.5.** *The notion of the tetrads* $\boldsymbol{e}$ *is sometimes introduced by another name (distortion field [26], vielbein [13]) or as a micro-deformation field in the microcontinuum theories [30, 69] or a Cartan's moving frame in a geometrical model [20].*

It is therefore usual to define metric components, as extension of the usual definitions

$$\widehat{\mathsf{G}}_{AB} = \mathbf{g}(\mathbf{e}^a_A e_a, \mathbf{e}^b_B e_b) = \mathbf{e}^a_A \mathbf{g}_{ab} \mathbf{e}^b_B, \tag{36}$$

where $\mathbf{g}$ is the metric tensor of the Euclidean space $\mathbb{E}^3$.

On the other hand, one can differentiate the vector base, and implicitly define an affine connection coefficients

$$\widehat{\nabla}_B e_C = \frac{\partial e_C}{\partial X^B} = \frac{\partial \mathbf{e}^c_C}{\partial X^B} e_c = \Big(\mathbf{e}^A_c \frac{\partial \mathbf{e}^c_C}{\partial X^B}\Big) e_A := \widehat{\Gamma}^A_{BC} e_A. \tag{37}$$

The connection may have both torsion and curvature. Furthermore, the connection is metric-compatible.

By construction, several cases may occur, it permits us to highlight the role of torsion and curvature tensors on the classification of continuum transformation.

*Holonomic transformation.* If the mapping $X \mapsto x$ is smooth and single-valued, the tetrads are usually the deformation gradient of the map with $\mathbf{e}^a_A = \partial x^a / \partial X^A$. Then it is straightforward to check that the torsion and curvature are equal to zero during an holonomic transformation. The same result is obtained if $F = \Psi$ in Theorem 4.3, or if $F = \Theta$ in Proposition 3.3.

*Non-holonomic transformation and torsion.* If $\mathbf{e}$ are single-valued but do not correspond to a deformation gradient, the induced manifold is a Weitzenböck manifold as in Theorem 4.3. In that sense, $\Psi$ plays the same roles as the tetrads $\mathtt{e}$. However, the presented approach differs on a crucial point: in the present model, the material manifold is a fibre bundle and the material transformation is a fibre morphism. Such a map is smooth and single-valued and is sufficient to define the induced metric and connection thanks to the concept of an Ehresmann connection. This point allows wide mathematical analysis and numerical simulation may be more comfortably handled.

*Non-holonomic transformation and curvature.* To go further, let us consider the multivaluedness of the tetrads. As a consequence, the connection has both torsion and curvature. This connection is metric compatible. However, the connection and metric are, generally, also multivalued. This could cause difficulties in performing consistent length measuring and parallel transport. In contrast, to achieve this goal the *scaled material model* in Section 3 is still driven by smooth fields (without additional degrees of freedom if (21) is used). Furthermore, a large class of manifolds have been observed, see Proposition 3.3.

### 4.3. Spin connection

As has been underlined previously, connection having both torsion and curvature cannot be obtained with single-valued tetrads. Another method consists of introducing an additional gauge field to give a connection [70] (see the discussion in [22]):

$$\widetilde{\Gamma}^A_{BC} = \mathbf{e}^A_c \partial_B \mathbf{e}^c_C + \mathbf{e}^A_c \overline{\Gamma}^c_{Bb} \mathbf{e}^b_C,$$

where the first term reduces to the Weitzenböck connection with non-zero torsion but zero curvature. The second term $\underline{\Gamma}^A_{BC} = \mathbf{e}^A_c \overline{\Gamma}^c_{Bb} \mathbf{e}^b_C$ has the role of a spin connection, with possibly non-zero torsion and/or non-zero curvature. Such a connection is metric compatible.

The similarity with (23) has to be underlined even if the overall approach is different. In $\Gamma^A_{BC} = \zeta \Theta^A_a \partial_A \Theta^a_C + (1-\zeta)\Theta^A_a \partial_B F^a_C$, the first term is the Weitzenböck connection, whereas the other $\Theta^A_a \partial_B F^a_C$ plays the role of a spin connection.

### 4.4. Comparison with Kröner–Lee decomposition

Lee and coworkers [68, 71], starting with the ideas from [14, 43] and the multiplicative decomposition of the deformation gradient $\mathbb{F} = \mathbb{F}_e \mathbb{F}_p$ (which was initially proposed by [10] and [17]), obtained some relations between torsion of the crystal connection and the elastic and plastic deformation gradients. The material connection here is metric compatible, with torsion but vanishing curvature. The work of [20] was inspired by this approach and introduced the slightly different method in which they identified the plastic deformation gradients

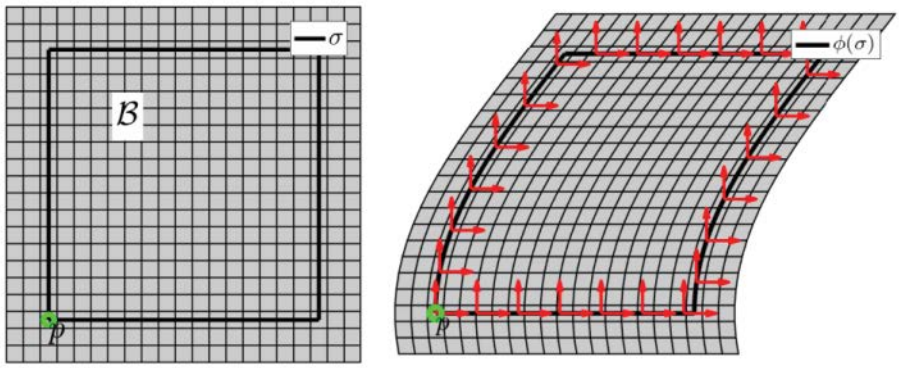


**Figure 4.** Left: Representation of the body $\mathscr{B}$. Cells are representations of $T\mathscr{B}$. A closed material loop $\sigma(t)$ is specified. This loop $\sigma$ is used throughout Section 5. Right: A defect-free current state in the ambient space $\mathbb{E}^2$.

as Cartan's moving frames to construct the appropriate material manifolds. Nevertheless, the requirement that the material manifold with an evolving connection (compatible with the metric) such that the frame field is everywhere parallel is not trivial.

The present model seems to be an alternative to the multiplicative decomposition $\mathbb{F} = \mathbb{F}_e\mathbb{F}_p$ generally used for elastoplastic transformation of a material. It is clear that the total gradient is $\Theta$ which controls stretch of microelements from the initial to final state. Elastic part is then the derivative of $\phi$ and, hence, $\mathbb{F}_p \sim F^{-1}\Theta$. This last expression obscures a crucial point: in the present model the intermediate configuration is not present. This concept is replaced by the consideration of vertical and horizontal tangent spaces that are the support for map linearisation on a vector field related to distinct quantities: $H(\mathscr{M})$ is related to the macroscopic vector field whereas $V(\mathscr{M})$ is related to the vector field associated with the microstructure (orientation of grains in a lattice, for example). Such interpretation avoids the standard intermediate configuration. More crucially, it is an alternative to the homogenisation process introduced recently [19]. In this latter work, as in the present paper, a scaling effect is introduced in order to replace the intermediate configuration. The point of view presented in Section 3 suffices to introduce several types of microstructural processes and defects in a unified geometrical formalism and with a reduced number of kinematical variables (in practice, the class of defects is wider than in Reina et al.'s approach).

## 5. Applications

In order to present the applications of the *scaled material model*, illustrations are restricted to in-plane motion in the Euclidean ambient space endowed with $\mathrm{g} = \delta$ and the trivial Levi-Civita connection $n = 0$. Hence, the body $\mathscr{B}$ is labelled by two Cartesian coordinates $(X^1, X^2)$ with respect to an affine frame $(O, e_1, e_2)$ on the plane, see Figure 4(left). A current state related to a defect-free transformation is represented in the ambient space $\mathbb{E}^2$ (Figure 4, right). As no defect is present, the parallel transport of a frame (red arrows) along a path $\phi(\sigma(t))$ does not change its ambient properties. However, material components of a parallel transported vector change along the path. On the other hand, the dragging of material vectors by the transformation is depicted by the change of size and form of the cells. This shape reveals the material metrics.

In Figure 5 another point of view is proposed where the transformation is presented in $\mathscr{B}$ by a pull-back operation. Here, the non-uniformity of the parallel transported frames is the manifestation of the material transformation.

For a more general transformation, for which the body contains defects, $\Upsilon^v$ is defined by (13) with condition (21). The prescribed maps $\phi$, $F = \phi_*$ and $\Theta$ are smooth, invertible and orientation preserving. Hence, for a given $\zeta$, these ingredients are used to define $\mathsf{G}$, $\Gamma$, $\mathsf{T}$, $\mathsf{R}$ and $\mathsf{Q}$ (see (19), (23), (24), (25) and (26), respectively). These Lagrangian tensors depend on the reference coordinates and are associated with fiber bundles on the body $\mathscr{B}$. In order to illustrate various types of defect, the parallel and rolling transports are complementary tools revealing the geometrical properties of the manifold (Section 2.3). However, their manifestations differ according to the chosen representation as was already observed by comparing Figures 4 and 5. Here we briefly present how such transports may be computed and illustrated.

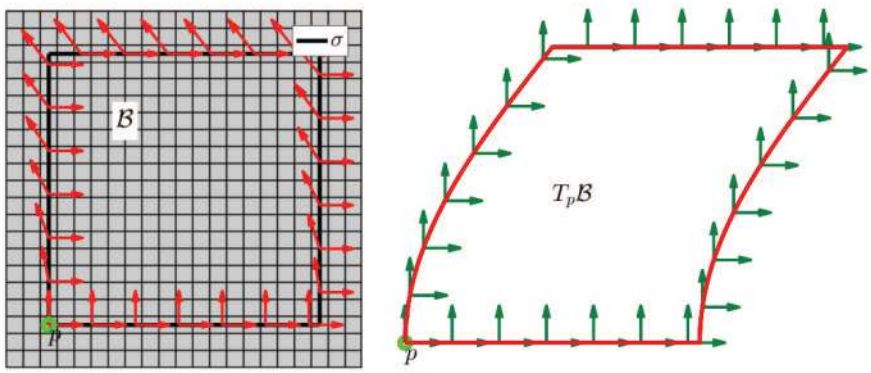


**Figure 5.** Left: The same defect-free current state as in Figure 4 but represented in $\mathscr{B}$. Right: Developing curve $\widetilde{\sigma}$ of $\sigma$ on $T_p\mathscr{B}$.

Let us first consider a point $p \in \mathscr{B}$ and a path $\sigma(t) = (X^A(t))$ on $\mathscr{B}$ parameterised by $t \in [0, 1]$ with $\sigma(0) = p$. The parameterisation $\sigma(t)$ generates a tangent vector field $\dot{\sigma}(t) = \dot{X}^A(t)\partial/\partial X^A$, with $dX^A = \dot{X}^A(t)\,dt$ defined for numerical purpose.

1. The *parallel transport* of a vector $Y^I e_I \in T_p\mathscr{B}$ along $\sigma$ is obtained by solving (4):

$$Y^I(t + dt) = Y^I(t) - \Gamma^I_{AJ}(\sigma(t))Y^J dX^A \quad \text{with } Y^I(0) = Y^I. \tag{38}$$

   A vector $Y^I(t)$ belongs to $T_{\sigma(t)}\mathscr{B}$. For illustration on $\mathbb{E}^2$, $F(\sigma(t))Y(t)$ is presented at $\phi(\sigma(t))$.
2. The *rolling transport* of the point $p + \widetilde{Y}^I e_I \in \mathscr{M}_p$ along $\sigma$ is the point $\sigma(t) + Y^I(t)e_I \in \mathscr{M}_{\sigma(t)}$ obtained by determining $Y(t) = (Y^I(t))$ solving (5):

$$Y^I(t + dt) = Y^I(t) - \Gamma^I_{AJ}(\sigma(t))Y^J dX^A - \delta^I_A dX^A \quad \text{with } Y^I(0) = \widetilde{Y}^I. \tag{39}$$

   Such a vector gives the coordinates of a point in the frame $(\sigma(t), e_1, \ldots, e_n)$ of $T_{\sigma(t)}\mathscr{B}$. Remember that $\mathscr{M}_p$ is $T_p\mathscr{B}$ viewed as an abstract affine space tangent to $\mathscr{B}$ at $p$. In particular, $\mathscr{M}_p \cap \mathscr{B} = \{p\}$.

This last transport is used to define two reciprocal transports of curves.

1. For a path $\sigma$ on $\mathscr{B}$, the *developing curve* is the curve $\widetilde{\sigma}$ on $T_p\mathscr{B}$ such that the rolling transport of $\widetilde{\sigma}(t) = p + \widetilde{Y}^I(t)e_I$ in $T_{\sigma(t)}\mathscr{B}$ is the origin of this tangent space, namely $\sigma(t)$ (a pictorial representation is given by Figure (6)). This curve is the curve drawn by the contact point of tangency of an affine space that rolls without slipping along $\sigma$, staying tangent to $\mathscr{B}$. It can be computed by searching the successive initial conditions $\widetilde{Y}(t)$ such that the coordinates of the rolling transport on $T_{\sigma(t)}\mathscr{B}$ are null. The procedure is as follows.
   Let $A(t)$ be the matrix solving $dA = -\mathcal{O}A$ along $\sigma$ with initial condition $A(0) = Id$ and $B(t)$ be the solution of $dB = -\mathcal{O}B - J$ along $\sigma$ with initial condition $B(0) = 0$. Then the solution of (5) along $\sigma$ with initial condition $Y(0)$ is $Y(t) = A(t)Y(0) + B(t)$. Now the developing curve is $\sigma(0) + \widetilde{Y}^I(t)e_I$ with $\widetilde{Y}(t)$ satisfying $0 = A(t)\widetilde{Y}(t) + B(t)$, i.e. $\widetilde{Y}(t) = -A^{-1}(t)B(t)$. Technically, one solves the equations on $A$ and $B$ by a numerical Euler scheme:

$$A^I_K(t + dt) = A^I_K(t) - \Gamma^I_{AJ}(\sigma(t))A^J_K(t)dX^A(t) \qquad \text{with } A(0) = Id, \tag{40}$$

$$B^I(t + dt) = B^I(t) - \Gamma^I_{AJ}(\sigma(t))B^J(t)dX^A(t) - \delta^I_A dX^A(t) \qquad \text{with } B(0) = 0. \tag{41}$$

   Then $\widetilde{Y}(t) = -A^{-1}(t)B(t)$ is plotted on $T_p\mathscr{B}$. The developing curve $\widetilde{\sigma}$ of $\sigma$ is presented on $T_p\mathscr{B}$ in Figure 5(right). On $T_p\mathscr{B}$, all the frames parallel-transported along $\sigma$ are equal (this holds true even for defective transformations).
2. The *driven curve* is the curve $\sigma$ on $\mathscr{B}$ whose developing curve is a given curve $\widetilde{\sigma}$ in $T_p\mathscr{B}$. The driven curve is unique if the initial point of $\widetilde{\sigma}$ is $p$. Indeed, comparison of two deformations could be done by fixing a curve $\widetilde{\sigma}$ in $T_p\mathscr{B}$ and comparing the two driven curves on $\mathscr{B}$.

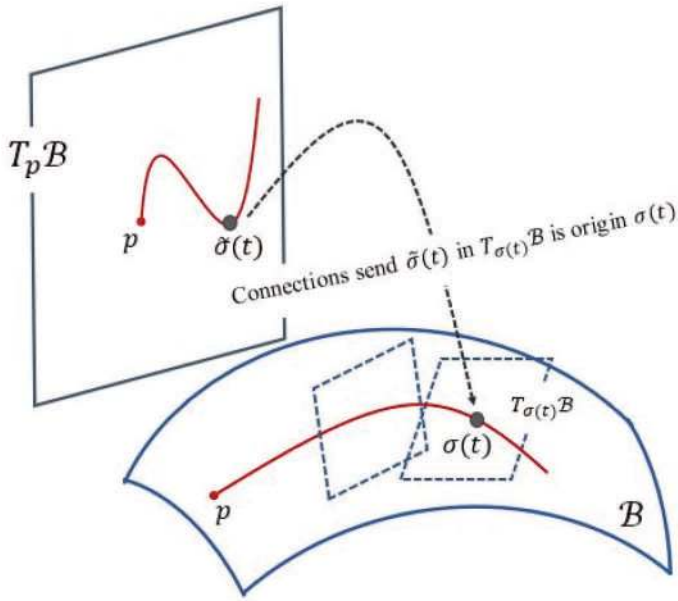


**Figure 6.** A pictorial representation of the developing curve.

This curve is obtained by solving a non-linear system of ODE. Let $\Gamma^I_{AJ}$ be the coefficients of the connection and $\widetilde{\sigma}(t) = p + \widetilde{Y}^I(t)e_I$ be a path in $T_p\mathscr{B}$ satisfying $\widetilde{Y}^I(0) = 0$. The driven curve $\sigma(t) = (X^A(t))$ and the matrix of the parallel transport $A(t)$ along $\sigma$ have to be computed simultaneously:

$$X^A(t+dt) - X^A(t) = \delta^A_I A^I_J(t)\big(\widetilde{Y}^J(t+dt) - \widetilde{Y}^J(t)\big) \tag{42}$$

$$A^I_J(t+dt) - A^I_J(t) = -\Gamma^I_{AK}(\sigma(t))A^K_J(t)(X^A(t+dt) - X^A(t)) \tag{43}$$

where $\Gamma^K_{AJ}(\sigma(t))$ is nothing else than $\Gamma^K_{AJ}(X^A(t))$. Initial guesses are $X^A(0) = 0$ and $A(0) = Id$. The driven curve can be plotted either on $\mathscr{B}$ or on $\phi(\mathscr{B})$.

Let us use $\mathcal{D} : (p, \sigma(t)) \to (p, \widetilde{\sigma}(t))$ to denote the application defining a developing curve. If $\widetilde{\sigma}$ is the developing curve of $\sigma$ on $\mathscr{B}$, then $\sigma$ is the driven curve of $\widetilde{\sigma}$. In other words, the application $(p, \widetilde{\sigma}(t)) \to (p, \sigma(t))$ defining a driven curve is $\mathcal{D}^{-1}$. Hence, the presence of a defect may be characterised on $T_p\mathscr{B}$ (by fixing a loop $\sigma$ and analysing the properties of $\widetilde{\sigma}$) or in $\mathscr{B}$ (by fixing a $\widetilde{\sigma}$ and checking the properties of the corresponding driven curve). These two methods are equivalent.

For a defect-free transformation, the image of the transformation given by the driven curve (Figure 5(right)) and by the embedding in the Euclidean space (Figure 4(right)) are the same up to a rigid motion. It is no longer true for a defective transformation as we show in the following examples.

### *5.1. Pure non-metric transformation*

Let us consider the map $\phi$ and its derivative $F$ as follows:

$$\begin{array}{rccl} \phi & X^1 & \to & x^1 = X^1 + h(X^2) \\ & X^2 & \to & x^2 = X^2 \end{array} \qquad F = \begin{pmatrix} 1 & f(X^2) \\ 0 & 1 \end{pmatrix}, \tag{44}$$

where $h$ is a $\mathscr{C}^2$-function $\mathscr{B} \to \mathbb{R}$ and, of course, $f(X^2) = \partial_2 h$. Suppose that $\Theta$ is identity, and then $\mathsf{G} = \delta$. The only non-zero connection coefficient is $\Gamma^1_{22} = (1-\zeta)\,\partial_2 f$ and, consequently, $\mathsf{T} = 0$. Direct computation shows that $\mathsf{R} = 0$. However, the connection is not metric-compatible as:

$$\nabla_2 \mathsf{G}_{12} = \nabla_2 \mathsf{G}_{21} = -(1-\zeta)\frac{\partial f}{\partial X^2} \tag{45}$$

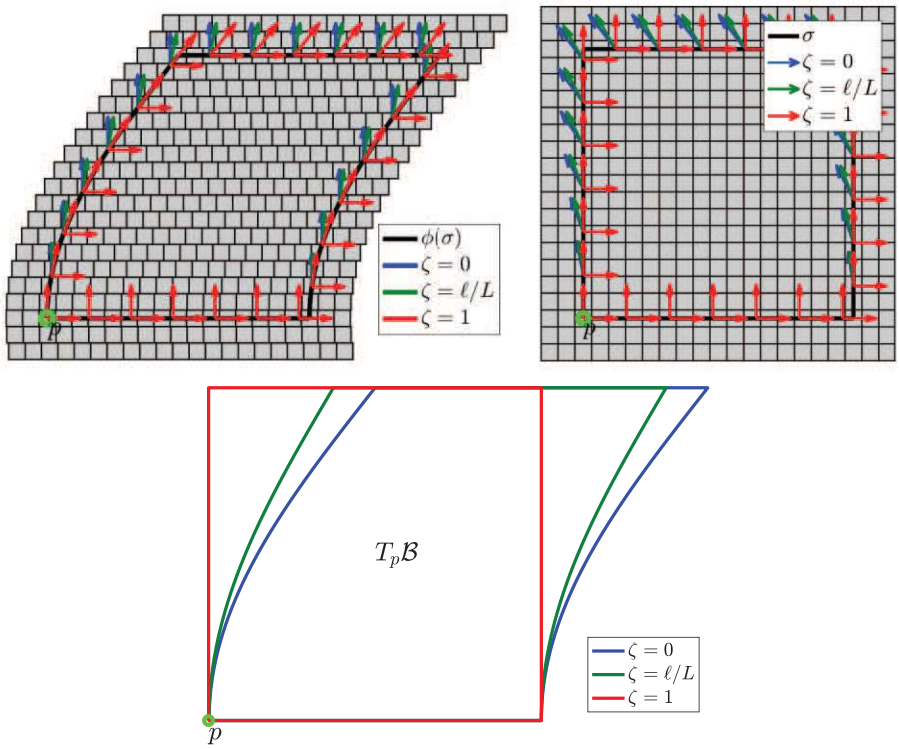


**Figure 7.** Numerical simulations of the transformation (44). The current state has no torsion and no curvature but the metric is not compatible with the induced connection. Top representation in $\mathbb{E}^3$ (right) and in $\mathscr{B}$ (left). The frame at $p$ is parallel-transported along $\sigma$. The bottom developing curve of $\sigma$ on $T_p\mathscr{B}$ obtained for various $\zeta$.

(the other components of $\mathbf{Q}$ are zero).

This situation is illustrated for various $\zeta$ in Figure 7 with

$$f(X^A) = \frac{\pi}{4} \sin\left(\frac{X^A}{8L}\pi\right), \tag{46}$$

of course $X^A = X^2$. Each cell is related to a microelement. As the relative placement of a microcell is controlled by $F$ the superposition of macro- and micro-stretch is graphically interpretable. The identity $\mathtt{G} = \delta$ supported by the local metric is clearly highlighted as the shape and size of cells are unchanged. This lattice representation is not sensitive to $\zeta$. A rigid translation of each microscopic layer is observed in the current configuration. The incompatibility of the gliding of macrocells with the metric of microelements is clearly quantified by $\nabla_2 \mathtt{G}_{12} \neq 0$. No voids or overlaps appear: this phenomenon is not intrinsically measured by $\mathbf{Q}$.

The parallel transport along $\sigma$ of a vector frame initially placed at $p$ is obtained by solving (38). It is observed that the vectors change along the loop even if no torsion and no curvature are present in the induced manifold. This phenomena is a direct repercussion of the non-standard connection which takes into consideration the transformation at both scales. After transportation along the closed loop the final vector coincides with the initial vector as no curvature is present. The parallel transport is highly sensitive to $\zeta$. If $\zeta = 0$, the effect of the micro-stretch is absent on the parallel transport. If $\zeta = 1$, the connection is compatible with the micro-metric, the parallel transport does not change locally the frame as $\Theta = Id$, however vectors are convected by $F$ if the transformation is presented in the ambient space.

The metric-incompatibility of the connection is also illustrated by the developing curve. If $\zeta = 0$, the developing curve coincides with $\phi(\sigma)$ up to a rigid motion. For $\zeta = 1$, the connection is compatible with the metric and the developing curves coincides with $\sigma$ as $\mathtt{G} = \delta$. In all the cases the developing curve are closed.

From an energetic point of view, it is clear that the reference and current state share the same internal energy. This is quantified by the preservation of metric, torsion and curvature between the two states. One may consider that in such infinite domain, the current state is obtained by a re-labeling of reference state. However, from

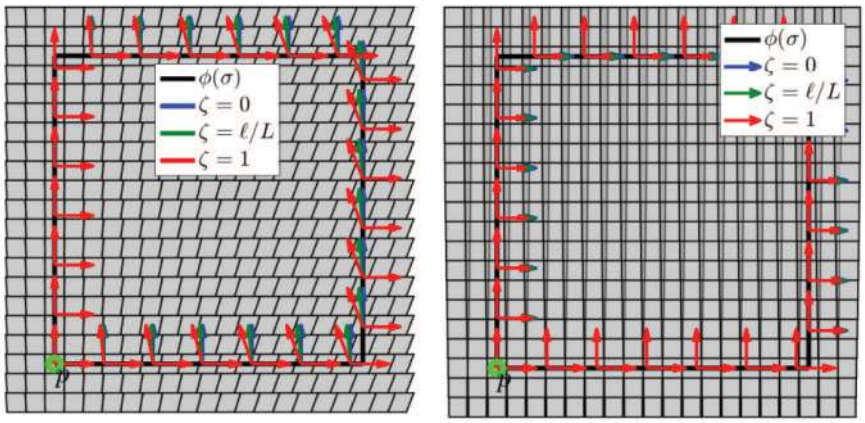


**Figure 8.** Representation in the ambient space of the current configuration for the transformations (47) (left) and (52) (right). There is no curvature but the non-zero components of the torsion are $\mathrm{T}^1_{12} = -\mathrm{T}^1_{21}$, the last metric is not compatible with the induced connection.

a mechanical point of view such re-organisation of material points involves some energy to cut inter-atomic interaction, even if the total energy involved for both cutting and re-connecting all atoms is null. Hence, from a physical point of view, this process is associated to a shift of energetic interaction but is also time-consuming. The non-metricity tensor $\mathsf{Q}$ is a geometrical candidate for measuring such non-elastoplastic processes.

### *5.2. Torsion with no curvature*

Let now consider a transformation given by

$$F = \begin{pmatrix} 1 & 0 \\ 0 & 1 \end{pmatrix} \qquad \Theta = \begin{pmatrix} 1 & \theta(X^1) \\ 0 & 1 \end{pmatrix}. \tag{47}$$

In such case, the metric tensor is

$$\mathtt{G} = \begin{pmatrix} 1 & \theta \\ \theta & 1+\theta^2 \end{pmatrix}. \tag{48}$$

The non-zero connection coefficient is now $\Gamma^1_{12} = \zeta\, \partial_1\theta$ and the torsion is no longer null. More precisely, the non-zero components of the torsion are

$$\mathsf{T}^1_{12} = -\mathsf{T}^1_{21} = \zeta \frac{\partial \theta}{\partial X^1}. \tag{49}$$

The curvature is zero, but the non-metricity tensor indicates

$$\nabla_1 \mathtt{G}_{22} = 2(1-\zeta)\theta\, \frac{\partial\, \theta}{\partial X^1} \qquad \nabla_1 \mathtt{G}_{12} = \nabla_1 \mathtt{G}_{21} = (1-\zeta)\frac{\partial\, \theta}{\partial X^1}. \tag{50}$$

An illustration is given in Figure 8(left) with $\theta$ taken as follows:

$$\theta(X^A) = \frac{\pi}{4} \cos\left(\frac{X^A}{4L}\pi\right). \tag{51}$$

The presence of edge dislocation with defects along $X^1$ is clearly observed.

Other types of dislocations may be obtained, with still $F = \mathbb{I}$ but

$$\Theta = \begin{pmatrix} 1+\theta(X^2) & 0 \\ 0 & 1 \end{pmatrix}. \tag{52}$$

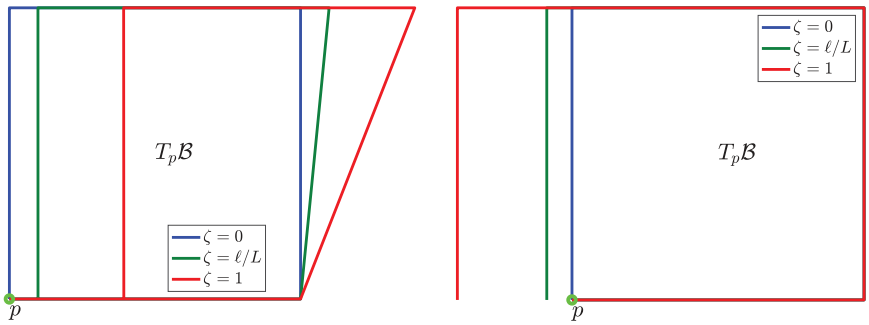


**Figure 9.** Developing curve $\widetilde{\sigma}$ obtained for various $\zeta$ and for the transformations (47) (left) and (52) (right).

Here

$$\mathtt{G} = \begin{pmatrix} (1+\theta)^2 & 0 \\ 0 & 1 \end{pmatrix} \tag{53}$$

and the only non-null connection coefficient is $\Gamma^1_{21} = \zeta\,(\partial_2\theta)/(1+\theta)$ leading to a non-null torsion,

$$\mathtt{T}^1_{21} = -\mathtt{T}^1_{12} = \zeta \frac{1}{1+\theta}\frac{\partial\theta}{\partial X^2}$$

what looks qualitatively similar to (49). The non-metricity has a unique non-null component:

$$\nabla_2\,\mathtt{G}_{11} = 2(1-\zeta)(1+\theta)\,\frac{\partial\,\theta}{\partial X^2}.$$

Last the curvature is still zero. Illustration is given in Figure 8(right) with $\theta$ still specified by (51) (with $X^A = X^2$). The pattern is clearly different to Figure 8(left). These two simulations show that several processes may be involved in order to create material with no curvature but a Burger vector along $X^1$. Even if the value of the torsion $\mathtt{T}^1_{12}$ is the same at a fixed point, for the two processes, the non-metricity tensor $\mathtt{Q}$ differs and provides information on the process involved.

Because $\phi$ is smooth and $\sigma$ is close, $\phi(\sigma)$ is close whatever the transformation (47) or (52). If a vector is parallel-transported along this closed loop (arrows in Figure 8) the final vector recovers its initial properties as it returns to the initial point (as the curvature is absent). Such procedure is not suitable for highlighting torsion of the manifold and, hence, revealing a distribution of dislocation in the defected material.

In Figure 9, the developing curve $\widetilde{\sigma}$ of $\sigma$ on $T_p\mathscr{B}$ is given. In that case, the curve $\widetilde{\sigma}$ is no longer closed if $\mathtt{T} \neq 0$ ($\zeta \neq 0$) and presents a gap along the $X^1$ direction. If computation is performed around $p$ along an infinitesimal material loop of size $\delta x^1 \times \delta x^2$ this gap coincides with $\mathtt{T}^1_{12}\delta x^1\delta x^2$. For such infinitesimal loop, it is a quantifier of dislocation density. Here the computation is performed on a finite domain and this gap on $\widetilde{\sigma}$ does not coincide with $\mathtt{T}^1_{12}\Delta x^1\Delta x^2$ (where $\Delta x^i$ are the size of the loop $\sigma$) as the torsion is not uniform in these simulations. It must be highlighted that even for such a finite loop, the directions $\dot{\sigma}$ at $p$ are unchanged. The developing curve preserves this signature if curvature is null as is commonly observed for infinitesimal domains. It can be seen as a characterisation of the absence of curvature in a finite domain.

It must be emphasised that the developing curve $\widetilde{\sigma}$ of a material curve $\sigma$ does not correspond to the heuristic process that follows, along the microstructure, the directions prescribed by a macroscopic loop. This principle is commonly presented as a methodology to define the Burger's vector over an infinitesimal material loop. It can be obtained by searching the path $\underline{\sigma}(t)$ (hereafter called the Burger's circuit) in $\mathscr{B}$ associated with coordinates $\underline{X}^A(t)$. The unknown $\underline{X}^A(t)$ is obtained by solving iteratively the process

$$(p, \sigma(t)) \xrightarrow{\mathcal{D}} (p, \tilde{\widetilde{\sigma}}(t)) \xrightarrow{\mathsf{D}^{-1}} (p, \underline{\sigma}(t)), \tag{54}$$

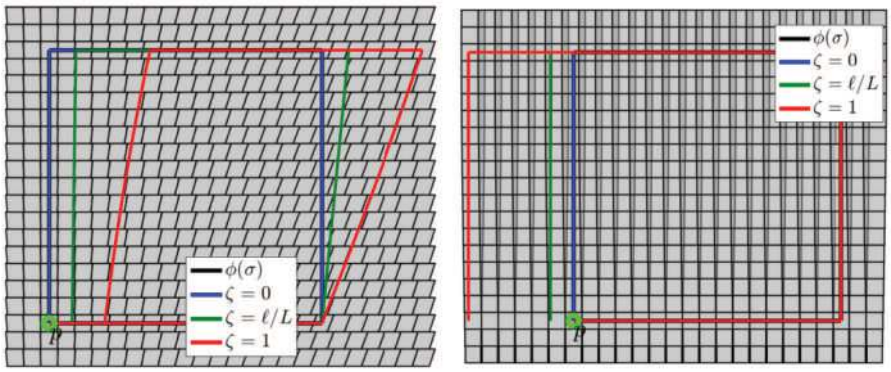


**Figure 10.** Burger's circuit $\underline{\sigma}$ obtained for various $\zeta$ and for the transformations (47) (left) and (52) (right) represented in the ambient space.

where $\mathsf{D}$ is the application defining the developing curve with connection of the base manifold $(\mathscr{B}, \mathsf{G}^h, \mathsf{L})$. As $\mathsf{D} \neq \mathcal{D}$, the Burger's circuit $\underline{\sigma}(t)$ is not $\sigma(t)$. In practice, the following Euler scheme is used to solve (54):

$$A^I_J(t+dt) = A^I_J(t) - \Gamma^I_{AK}(\underline{\sigma}(t))A^K_J(t)\underline{dX}^A(t) \qquad \text{with } A(0) = Id, \tag{55}$$

$$d\tilde{\tilde{Y}}(t) = A(t)^{-1}dX(t) \qquad \text{with } d\tilde{Y}(0) = dX(0), \tag{56}$$

$$\mathsf{A}^I_J(t+dt) = \mathsf{A}^I_J(t) - \mathsf{L}^I_{AK}(\underline{\sigma}(t))\mathsf{A}^K_J(t)\underline{dX}^A(t) \qquad \text{with } \mathsf{A}(0) = Id, \tag{57}$$

$$\underline{dX}(t) = \mathsf{A}(t)d\tilde{\tilde{Y}}(t) \qquad \text{with } \underline{dX}(0) = dX(0), \tag{58}$$

$$\underline{X}(t+dt) = \underline{X}(t) + \underline{dX}(t) \qquad \text{with } \underline{X}(0) = X(0), \tag{59}$$

Illustration is given in Figure 10 for the two transformations. If $\zeta = 1$, the result is equivalent to the standard illustration of a Burger's circuit on a RC manifold (with $\zeta = 0$ and for zero curvature $\underline{\sigma}(t) = \sigma(t)$). The present *scaled material model* enables this effect to be weighted if $\zeta \neq 1$.

In Figure 10, the orientation $\dot{\underline{\sigma}}$ is not preserved after the finite loop: $\Delta\dot{\underline{\sigma}} = \dot{\underline{\sigma}}(1) - \dot{\underline{\sigma}}(0) \neq 0$ in contrast to what was observed on the developing curve. In other words, on a finite Burger's circuit $\Delta\dot{\underline{\sigma}} = 0$ is not a signature of the absence of curvature. It must also be observed that the gap between the initial and final point of the path $\Delta\underline{\sigma} = \underline{\sigma}(1) - \underline{\sigma}(0)$ is different to $\Delta\widetilde{\sigma} = \widetilde{\sigma}(1) - \widetilde{\sigma}(0)$. The last numerical simulations show that $\Delta\underline{\sigma}$ changes if traveling along $\sigma$ is performed clockwise or counterclockwise. This confirms that the Burger's circuit is not a topologically invariant measure of defect density. In contrast, $\Delta\widetilde{\sigma}$ is unchanged and looks more robust for a quantification of the defect density.

### *5.3. Curvature with no torsion*

Let us consider a kinematic transformation specified by the following tensors:

$$F = \begin{pmatrix} 1 & f(X^2) \\ 0 & 1 \end{pmatrix} \qquad \Theta = \begin{pmatrix} 1+\theta(X^1) & 0 \\ 0 & 1 \end{pmatrix}. \tag{60}$$

Note that both of them may be defined as a total derivative of a $\mathscr{B} \to \mathbb{E}^3$ map. The metric is of the form (53). The non-null connection coefficients are $\Gamma^1_{11} = \zeta(\partial_1\theta)/(1+\theta)$ and $\Gamma^1_{22} = (1-\zeta)(\partial_2 f)/(1+\theta)$ then the torsion is null. The non-zero components of the curvature are

$$\mathsf{R}^1{}_{212} = -\mathsf{R}^1{}_{221} = -\left(\frac{1-\zeta}{1+\theta}\right)^2 \frac{\partial f}{\partial X^2}\frac{\partial \theta}{\partial X^1}.$$

The non-metricity tensor has the following non-null components:

$$\nabla_1 \mathsf{G}_{11} = 2(1-\zeta)(1+\theta)\frac{\partial\,\theta}{\partial X^1}, \quad \nabla_2 \mathsf{G}_{12} = \nabla_2 \mathsf{G}_{21} = -(1-\zeta)(1+\theta)\frac{\partial f}{\partial X^2}.$$

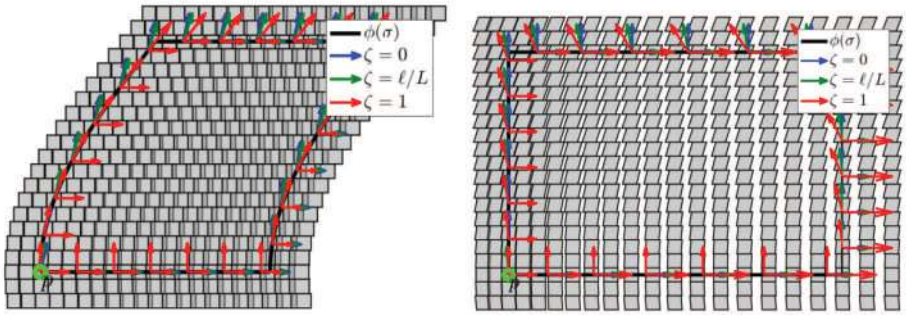


**Figure 11.** Representation in the ambient space of the transformation (60) (left) and (61) (right). There is no torsion but the non-zero components of the curvature are $\mathrm{R}^1{}_{212} = -\mathrm{R}^1{}_{221}$ and the metric is not compatible with the induced connection.

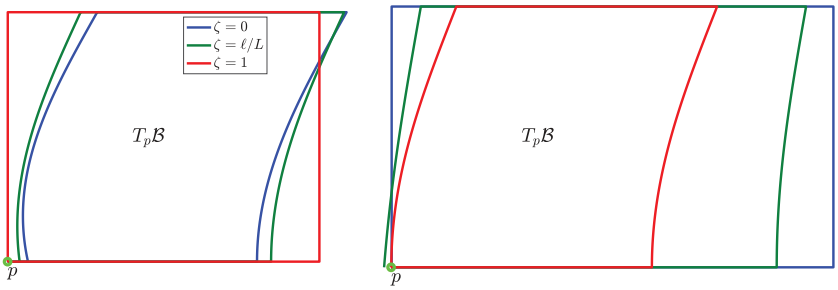


**Figure 12.** Developing curve $\widetilde{\sigma}$ obtained for various $\zeta$ and for the transformations (60) (left) and (61) (right).

Numerical simulation is given in Figure 11(left) with $f(X^2)$ and $\theta(X^1)$ specified by (46) and (51), respectively.

As for the example related to torsion, some other process may be involved in order to obtain the same type of curvature. Indeed, consider the transformation

$$F = \begin{pmatrix} 1 + f(X^1) & 0 \\ 0 & 1 \end{pmatrix} \qquad \Theta = \begin{pmatrix} 1 & \theta(X^2) \\ 0 & 1 \end{pmatrix}. \tag{61}$$

for which the metric is of the same form as (48). The non-null connection coefficients are $\Gamma^1_{11} = (1-\zeta)\partial_1 f$ and $\Gamma^1_{22} = \zeta\partial_2\theta$ then the torsion is null. The non-zero components of the curvature are

$$\mathsf{R}^1{}_{212} = -\mathsf{R}^1{}_{221} = (1-\zeta)\zeta\frac{\partial f}{\partial X^1}\frac{\partial \theta}{\partial X^2}.$$

The non-metricity has the following non-null components:

$$\nabla_1 \mathsf{G}_{11} = -2(1-\zeta)\frac{\partial f}{\partial X^1}, \quad \nabla_1 \mathsf{G}_{12} = \nabla_1 \mathsf{G}_{21} = -(1-\zeta)\,\theta\,\frac{\partial f}{\partial X^1}$$
$$\nabla_2 \mathsf{G}_{22} = 2(1-\zeta)\theta\frac{\partial\,\theta}{\partial X^2}, \quad \nabla_2 \mathsf{G}_{12} = \nabla_2 \mathsf{G}_{21} = (1-\zeta)\frac{\partial\,\theta}{\partial X^2}.$$

The corresponding illustration (Figure 11, right) exhibits a highly different pattern to Figure 11(left) even if the same components of the curvature are involved. For both simulations, a frame initially placed at $p$ is parallel-transported along $\sigma$ by solving (38). For both transformations, the initial (vertical) vector $Y(0)$ and last vector $Y(1)$ differ if the curvature is not zero. Indeed, for an infinitesimal loop of side $\delta x^1 \times \delta x^2$ the horizontal gap of $\Delta Y = Y(0) - Y(1)$ is measured by $\mathsf{R}^1_{212}Y^2\delta x^1\delta x^2$. For an infinitesimal domain, it is a signature of the curvature and then of the disclination densities. At a macroscopic point of view, it is still measurable by such a gap.

The developing curve $\widetilde{\sigma}$ is presented for the two transformations in Figure 12. Here the computation is performed for finite loop and $\widetilde{\sigma}$ is no longer close as if the manifold presents non-null torsion. For an infinitesimal loop, the computation of a such gap $\Delta\widetilde{\sigma} = \widetilde{\sigma}(1) - \widetilde{\sigma}(0)$ shows that $\Delta\widetilde{\sigma} = \mathcal{O}(\delta x^3)$ in the presence of curvature.

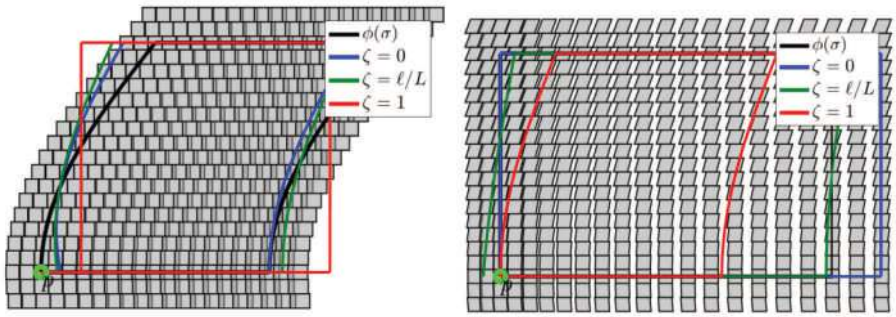


**Figure 13.** Burger's circuit $\underline{\sigma}$ obtained for various $\zeta$ and for the transformations (60) (left) and (61) (right) represented in the ambient space.

In other words, for an infinitesimal loop $\Delta Y$ is preponderant to $\Delta\widetilde{\sigma}$. However, for a finite loop this hierarchy is broken as both $\Delta Y$ and $\Delta\widetilde{\sigma}$ are non-negligible. As $\Delta\widetilde{\sigma}$ is of the same order of magnitude in the presence of curvature or torsion (Figure 9), it is impossible to confirm that no torsion is present in such a finite domain. In other words, $\Delta\widetilde{\sigma}$ observation on a finite domain is not able to discriminate the density of dislocations if some disclinations are present.

The Burger's circuits $\underline{\sigma}$ obtained by (54) are presented in Figure 13. As in the previous example (*i*) the gap of Burger's circuit differs quantitatively from the gap observed for the developing curve (*ii*) the vectors $\underline{\dot{\sigma}}(1)$ and $\underline{\dot{\sigma}}(0)$ are distinct. Hence, this Burger's circuit associated with a finite loop is not able to discriminate whether defects are associated to torsion only, curvature only or both of them together. From this point of view, the analysis of the developing curve has the advantage of discriminating between the presence and absence of curvature by considering $\Delta\widetilde{\sigma}$.

## 6. Conclusion

In order to model a material transformation that takes into consideration the change and eventually creations of defects, a geometrical approach has been posited. In this context, such transformation is considered as a fibre morphism, or so-called bundle map, from the appropriate fibre bundle of the material manifold to the Euclidean space. The method is based on the concepts of Ehresmann connection and solder form. The induced connection $N$ and metric $\mathtt{G}$ are first described, then curvature, torsion and non-metricity of the connection may be obtained. The more straightforward method consists of studying $\mathscr{M} \to T\mathbb{E}^3$. It has been proven that this approach is not able to introduce curvature, even in the case of non-linear maps.

The main idea to introduce rich enough transformations consists of considering that the bundle supporting the transformation is $V\mathscr{M}$, which is the vertical tangent bundle of $\mathscr{M}$. In this article, the transformations $\Upsilon^v : V\mathscr{M} \to VT\mathbb{E}^3$ are restricted to the case of linear micro-structure, meaning that $\mathscr{M}$ is isomorphic to $T\mathscr{B}$.

This assertion does not constrain entirely $T\mathscr{M}$ and is a geometrical modelling of the misfit between the microscopic and macroscopic states of the material, it is a *scaled material model*. Technically, this misfit is taken into account by the connections that illustrate, through its torsion, curvature and non-metricity, the presence of various material defects. Here the material is described by a body $\mathscr{B}$ having a microstructure $\mathscr{M}$. In such a way, each geometrical quantity may be measured or computed on the same material locus: the body $\mathscr{B}$. In all cases, the current state is obtained by a pull-back operation that prescribed an *induced* geometry on $\mathscr{B}$.

As the *scaled material model* embraces various underlying points of view (microscopic, macroscopic and macroscopic interpretation of a microscopic phenomena) the standard parallel transport is not sufficient. For this purpose, various interpretations, including the rolling without slipping transport and the developing curve, have been exhibited and illustrated in order to link the mathematical tools to the mechanical processes.

Such a *scaled material model* is parameterised by single-valued and smooth fields. It is the case for the induced (linear) connection $\Gamma$ and metric $\mathtt{G}$ (then for torsion or curvature) but also for the point and vector maps $\phi$ and $\Theta$. This feature distinguishes the present model from other known theories referring to the non-holonomic principle. It allows mathematical analysis and numerical simulation taking into account both scales.

The non-metricity of the connection can be considered as *the price to be paid* by the *scaled material model* to overcome multivalued fields. However, through this modelling, the non-metricity reveals the process involved

to obtain a defective medium. Analysing more deeply this mechanical interpretation is among the possible objectives of future work.

The restriction of the bundle map $\Upsilon$ to any element of $V\mathscr{M}$ is imposed by the transformation $\Upsilon^{v}$. Accordingly, specifying the completed bundle map $\Upsilon$ is somehow free. In the present work, a family of bundle maps $\Upsilon$ is considered by introducing just a unique scalar $\zeta$. This choice is sufficient to illustrate the presence of various defect types and avoids adding new unknown fields in the theory. In the present example, $\zeta$ gives a weight of macro- and micro-effects in a linear way, but other formulations (leading, for instance, to non-linear connection) are possible. It must be noted that the choice of such completion may reveal some interesting physical interpretations that are beyond the scope of this paper (in particular, for multi-physical problems).

Numerical simulations are presented and show how bridges are built between microscopic defects and macroscopic observations. It is the occasion to underline that for a given density of disclinations, the characterisation of the possible presence of dislocations is not attainable by macroscopic observations (at least with the $\zeta$-family of bundle maps$\Upsilon$ chosen in the present case).

The present model is currently purely kinematic. However, this first step was indispensable to consider full mechanical problems afterwards. (1) Staying on this kinematic approach, other possible extensions $\Upsilon$ (than the $\zeta$-family) may be explored in order to take into account specific microstructured materials such as nanomaterials. (2) The study of the solder form turns out to be another interesting subject. (3) Another possible step consists of considering an energetic counterpart in order to define the equilibrium laws of such a model. (4) Note that the present *scaled material model* is kinematically non-linear, and a linearisation may be the occasion to furnish some meaningful explicit solutions. (5) Another possible issue consists of introducing time into the Galilean or Lorentzian framework.


## Acknowledgement

The authors are very grateful to Professor Lalaonirina Rakotomanana for careful and thoughtful comments on this work.

## Funding

This work was supported in part by the Henri Lebesgue Center. The authors also gratefully acknowledge IRMAR - CNRS UMR 6625 for providing financial support.


### Notes

1. In this proof, we have used the fact that $\mathfrak{M}$ and $\mathfrak{N}$ are arbitrary differential manifolds, for any vector $u, v$ on $\mathfrak{M}$ and differential map $h$: $\mathfrak{M} \to \mathfrak{N}$, then $h_*[u, v] = [h_*u, h_*v]$; see Chapter 5.3.2 in [51].


### ORCID iD

Van Hoi Nguyen https://orcid.org/0000-0002-1663-2817


### References


[1] Cartan, É. Sur une généralisation de la notion de courbure de riemann et les espaces à torsion. *C R Acad Sci Paris* 1922; 174: 593–595.

[2] Cosserat, E, and Cosserat, F. *Sur la théorie des corps déformables*. Paris: Dunod, 1909.

[3] Burgers, J, and Burgers, W. Dislocations in crystal lattices. In Eirich, FR (ed.) *Rheology*. New York: Academic Press, 1956, pp. 141–199.

[4] Volterra, V. Sur l'équilibre des corps élastiques multiplement connexes. *Ann Sci École Norm Sup (3)* 1907; 24: 401–517.

[5] Weyl, H. Reine Infinitesimalgeometrie. *Math Z* 1918; 2(3–4): 384–411.

[6] Cartan, É. Sur les variétés à connexion affine et la théorie de la relativité généralisée (première partie). *Ann Sci École Norm Sup (3)* 1923; 40: 325–412.

[7] Cartan, É. Sur les variétés à connexion affine, et la théorie de la relativité généralisée (première partie) (Suite). *Ann Sci École Norm Sup (3)* 1924; 41: 1–25.

[8] Cartan, É. Sur les variétés à connexion affine, et la théorie de la relativité généralisée (deuxième partie). *Ann Sci École Norm Sup (3)* 1925; 42: 17–88.

[9] Kondo, K. *Geometry of elastic deformation and incompatibility. Memoirs of the unifying study of the basic problems in engineering sciences by means of geometry. Vol. I*. Tokyo: Gakujutsu Bunken Fukyu-Kai, 1955.

[10] Bilby, BA, Bullough, R, and Smith, E. Continuous distributions of dislocations: A new application of the methods of non-Riemannian geometry. *Proc R Soc Lond A* 1955; 231: 263–273.

[11] Kröner, E. Allgemeine Kontinuumstheorie der Versetzungen und Eigenspannungen. *Arch Rat Mech Anal* 1960; 4: 273–334.

[12] Kröner, E. Physics of defects. In: *Continuum Theory of Defects*, Less houches, session xxxv, 1980. Amsterdam: North-Holland, 1981.

[13] Katanaev, M. Geometric theory of defects. *Phys Usp* 2005; 48(7): 675–701.

[14] Noll, W. Materially uniform simple bodies with inhomogeneities. *Arch Rat Mech Anal* 1967/68; 27: 1–32.

[15] Rakotomanana, LR. Contribution à la modélisation géométrique et thermodynamique d'une classe de milieux faiblement continus. *Arch Rat Mech Anal* 1998; 141(3): 199–236.

[16] Epstein, M, and Segev, R. Geometric aspects of singular dislocations. *Math Mech Solids* 2014; 19(4): 337–349.

[17] Lee, E, and Liu, D. Finite-strain elastic–plastic theory with application to plane-wave analysis. *J Appl Phys* 1967; 38: 19–27.

[18] Yavari, A, and Goriely, A. Weyl geometry and the nonlinear mechanics of distributed point defects. *Proc R Soc Lond Ser A Math Phys Eng Sci* 2012; 468(2148): 3902–3922.

[19] Reina, C, Schlömerkemper, A, and Conti, S. Derivation of $\mathbf{F} = \mathbf{F}^{\mathrm{e}}\mathbf{F}^{\mathrm{p}}$ as the continuum limit of crystalline slip. *J Mech Phys Solids* 2016; 89: 231–254.

[20] Yavari, A, and Goriely, A. Riemann-Cartan geometry of nonlinear dislocation mechanics. *Arch Rat Mech Anal* 2012; 205(1): 59–118.

[21] Kleinert, H. *Multivalued Fields in Condensed Matter, Electromagnetism, and Gravitation*. Hackensack, NJ: World Scientific, 2008.

[22] Rakotomanana, LR. *Covariance and Gauge Invariance in Continuum Physics: Application to Mechanics, Gravitation, and Electromagnetism* (*Progress in Mathematical Physics*, Vol. 73). Cham: Birkhäuser/Springer, 2018.

[23] Kleinert, H. Nonholonomic mapping principle for classical and quantum mechanics in spaces with curvature and torsion. *Gen Relativ Gravitat* 2000; 32(5): 769–839.

[24] Futhazar, G, Le Marrec, L, and Rakotomanana, L. Covariant gradient continua applied to wave propagation within defective material. *Arch Appl Mech* 2014; 84(9–11): 1339–1356.

[25] Peshkov, I, Romenski, E, and Dumbser, M. Continuum mechanics with torsion. *Contin Mech Thermodyn* 2019; 31(5): 1517–1541.

[26] Peshkov, I, and Romenski, E. A hyperbolic model for viscous Newtonian flows. *Contin Mech Thermodyn* 2016; 28(1–2): 85–104.

[27] Dumbser, M, Peshkov, I, and Romenski, E. A unified hyperbolic formulation for viscous fluids and elastoplastic solids. In: *Theory, Numerics and Applications of Hyperbolic Problems. II* (*Springer Proceedings in Mathematics and Statistics*, Vol. 237). Cham: Springer, 2018, pp. 451–463.

[28] Eringen, AC, and Suhubi, ES. Nonlinear theory of simple micro-elastic solids. I. *Internat J Engrg Sci* 1964; 2: 189–203.

[29] Suhubi, ES, and Eringen, AC. Nonlinear theory of micro-elastic solids. II. *Internat J Engrg Sci* 1964; 2: 389–404.

[30] Mindlin, RD. Micro-structure in linear elasticity. *Arch Rat Mech Anal* 1964; 16: 51–78.

[31] Polizzotto, C. A second strain gradient elasticity theory with second velocity gradient inertia âŁ“ part I: Constitutive equations and quasi-static behavior. *Int J Solids Struct* 2013; 50(24): 3749–3765.

[32] Forest, S. Micromorphic approach for gradient elasticity, viscoplasticity, and damage. *J Eng Mech* 2009; 135(3): 117–131.

[33] Grammenoudis, P, and Tsakmakis, C. Micromorphic continuum. Part I: Strain and stress tensors and their associated rates. *Int J Non-Lin Mech* 2009; 44(9): 943.

[34] Ghiba, ID, Neff, P, Madeo, A, et al. The relaxed linear micromorphic continuum: existence, uniqueness and continuous dependence in dynamics. *Math Mech Solids* 2015; 20(10): 1171–1197.

[35] Madeo, A, Neff, P, Ghiba, ID, et al. Band gaps in the relaxed linear micromorphic continuum. *ZAMM Z Angew Math Mech* 2015; 95(9): 880–887.

[36] Madeo, A, Barbagallo, G, Collet, M, et al. Relaxed micromorphic modeling of the interface between a homogeneous solid and a band-gap metamaterial: new perspectives towards metastructural design. *Math Mech Solids* 2018; 23(12): 1485–1506.

[37] Neff, P, and Forest, S. A geometrically exact micromorphic model for elastic metallic foams accounting for affine microstructure. Modelling, existence of minimizers, identification of moduli and computational results. *J Elasticity* 2007; 87(2–3): 239–276.

[38] Yavari, A, Marsden, JE, and Ortiz, M. On spatial and material covariant balance laws in elasticity. *J Math Phys* 2006; 47(4): 042903.

[39] Yavari, A, and Marsden, JE. Covariant balance laws in continua with microstructure. *Rep Math Phys* 2009; 63(1): 1–42.

[40] Yavari, A, and Goriely, A. Riemann-Cartan geometry of nonlinear disclination mechanics. *Math Mech Solids* 2013; 18(1): 91–102.

[41] Epstein, M, and Elżanowski, M. Material inhomogeneities and their evolution: A geometric approach. In: *Interaction of Mechanics and Mathematics*. Berlin: Springer, 2007.

[42] Rougée, P. *Mécanique des grandes transformations*, (*Mathématiques & Applications (Berlin) [Mathematics & Applications]*, Vol. 25). Berlin: Springer-Verlag, 1997.

[43] Wang, CC. On the geometric structures of simple bodies. A mathematical foundation for the theory of continuous distributions of dislocations. *Arch Rat Mech Anal* 1967/68; 27: 33–94.

[44] Iliev, BZ. Fibre bundle formulation of nonrelativistic quantum mechanics. I. Introduction. The evolution transport. *J Phys A* 2001; 34(23): 4887–4918.

[45] Romano, G. Continuum mechanics on manifolds. *Lecture Notes*, University of Naples Federico II, Naples, Italy, 2007; pp. 1–695.
[46] Epstein, M. *The Elements of Continuum Biomechanics*. New York: John Wiley & Sons, 2012.
[47] Bradlyn, B, and Read, N. Low-energy effective theory in the bulk for transport in a topological phase. *Phys Rev B* 2015; 91: 125303.
[48] Lychev, S, Koifman, K, Petrenko, A, et al. Modeling and optimization for oriented growing solids. In: *2020 15th International Conference on Stability and Oscillations of Nonlinear Control Systems (Pyatnitskiy's Conference) (STAB)*, pp. 1–4.
[49] Hélein, F. Manifolds obtained by soldering together points, lines, etc. *arXiv preprint arXiv:0904.4616*, 2009.
[50] Kolev, B, and Desmorat, R. Objective rates as covariant derivatives on the manifold of riemannian metrics. *arXiv preprint arXiv:2106.01126*, 2021.
[51] Nakahara, M. *Geometry, Topology and Physics*. (2nd ed.) (*Graduate Student Series in Physics*). Bristol: Institute of Physics, 2003.
[52] Epstein, M. *The Geometrical Language of Continuum Mechanics*. Cambridge: Cambridge University Press, 2010.
[53] Epstein, M. *Differential Geometry: Basic Notions and Physical Examples*. Cham: Springer, 2014.
[54] Bao, D, Chern, SS, and Shen, Z. *An Introduction to Riemann-Finsler Geometry* (*Graduate Texts in Mathematics*, Vol. 200). New York: Springer-Verlag, 2000.
[55] Bucataru, I, and Miron, R. Applications to dynamical systems. In: *Finsler-Lagrange Geometry*. Bucharest: Editura Academiei Române, 2007.
[56] Pfeifer, C. *The Finsler Spacetime Framework: Backgrounds for Physics Beyond Metric Geometry*. PhD Thesis, Hamburg University, 2013.
[57] Bejancu, A. *Finsler Geometry and Applications* (*Ellis Horwood Series: Mathematics and Its Applications*). New York: Ellis Horwood, 1990.
[58] Kondo, K. Non-riemannian and finslerian approaches to the theory of yielding. *Int J Eng Sci* 1963; 1(1): 71–88.
[59] Saczuk, J. On the role of the Finsler geometry in the theory of elasto-plasticity. *Rep Math Phys* 1997; 39(1): 1–17.
[60] Fu, MF, Saczuk, J, and Stumpf, H. On fibre bundle approach to a damage analysis. *Internat J Engrg Sci* 1998; 36(15): 1741–1762.
[61] Stumpf, H, and Saczuk, J. A generalized model of oriented continuum with defects. *ZAMM Z Angew Math Mech* 2000; 80(3): 147–169.
[62] Clayton, JD. On Finsler geometry and applications in mechanics: Review and new perspectives. *Adv Math Phys* 2015; 11: 828475.
[63] Clayton, JD. Generalized Finsler geometric continuum physics with applications in fracture and phase transformations. *Z Angew Math Phys* 2017; 68(1): 9.
[64] Clayton, J. Finsler geometry of nonlinear elastic solids with internal structure. *J Geom Phys* 2017; 112: 118–146.
[65] Yajima, T, and Nagahama, H. Connection structures of topological singularity in micromechanics from a viewpoint of generalized Finsler space. *Ann Phys* 2020; 532(12): 2000306.
[66] Bucataru, I, and Miron, R. Nonlinear connections for nonconservative mechanical systems. *Rep Math Phys* 2007; 59(2): 225–241.
[67] Yajima, T, and Nagahama, H. KCC-theory and geometry of the Rikitake system. *J Phys A* 2007; 40(11): 2755–2772.
[68] Le, KC, and Stumpf, H. On the determination of the crystal reference in nonlinear continuum theory of dislocations. *Proc R Soc Lond Ser A Math Phys Eng Sci* 1996; 452(1945): 359–371.
[69] Eringen, AC. *Microcontinuum Field Theories. I. Foundations and Solids*. New York: Springer-Verlag, 1999.
[70] Obukhov, YN, Ponomariev, VN, and Zhytnikov, VV. Quadratic Poincaré gauge theory of gravity: A comparison with the general relativity theory. *Gen Relativ Gravitat* 1989; 21(11): 1107–1142.
[71] Le, K, and Stumpf, H. Nonlinear continuum theory of dislocations. *Int J Eng Sci* 1996; 34(3): 339–358.
[72] Choquet-Bruhat, Y, DeWitt-Morette, C, and Dillard-Bleick, M. *Analysis, Manifolds and Physics* (2nd ed.). Amsterdam: North-Holland, 1982.

## Appendix

### *A.1. RC manifold*

This appendix is a review of basic contents concerning RC geometry. All details can be found in the standard textbooks [22, 51, 52, 72].

On a manifold $\mathscr{B}$, one considers a metric tensor $\mathbf{g}$, its tangent space $T\mathscr{B}$ and its space $\mathfrak{X}(\mathscr{B})$ of $\mathscr{C}^\infty$ vector fields.

**Definition A.1 (Covariant derivative).** *Covariant derivative on $\mathscr{B}$ is an operation*

$$\begin{array}{rccc} \nabla \ : & \mathfrak{X}(\mathscr{B}) \times \mathfrak{X}(\mathscr{B}) & \to & \mathfrak{X}(\mathscr{B}) \\ & (u, v) & \to & \nabla_u v \end{array}$$

*which satisfies the following conditions,*

$$\begin{aligned} \nabla_u(v+w) &= \nabla_u v + \nabla_u w, & \nabla_{(fu)} v &= f\nabla_u v, \\ \nabla_{u+v} w &= \nabla_u z + \nabla_v w, & \nabla_u(fv) &= u[f]v + f\nabla_u v, \end{aligned} \tag{62}$$

*where $f \in \mathscr{C}^\infty(\mathscr{B})$ and $v[f]$ is the directional derivative of $f$ along the vector field $v$. Employing $(x^a)$ as a coordinate system on $\mathscr{B}$, one has $v[f] = v^a \partial_a f$ and*

$$\nabla_{\partial_a} \partial_b = \Gamma^c_{ab} \partial_c, \tag{63}$$

*where $\Gamma^c_{ab}$ are the Christoffel symbols and $(\partial_a) = (\partial/\partial x^a)$ is the natural base of the tangent space corresponding to the coordinate chart $(x^a)$. The Christoffel symbols specify how the basis vectors change from point to point.*

As the covariant derivative must not depend on the chosen coordinate, under a coordinate transformation $x^a \mapsto \tilde{x}^i = \tilde{x}^i(x^a)$ its Christoffel symbols must transform as

$$\widetilde{\Gamma}^k_{ij} = \frac{\partial x^b}{\partial \tilde{x}^i} \frac{\partial x^c}{\partial \tilde{x}^j} \frac{\partial \tilde{x}^k}{\partial x^a} \Gamma^a_{bc} + \frac{\partial^2 x^a}{\partial \tilde{x}^i \partial \tilde{x}^j} \frac{\partial \tilde{x}^k}{\partial x^a}. \tag{64}$$

Verifying that an object is a covariant derivative can be done by confirming that its Christoffel symbols are smooth functions satisfying the transformation rule (64). This implies that from a given covariant derivative $\nabla$, one obtains a linear connection $N$ on $T\mathscr{B}$ as defined in (2.2) where $N^i_a(x,y) = \Gamma^i_{aj}(x) y^j$. The usual formulations for torsion and curvature are as follows.

**Definition A.2 (Torsion).** *The torsion tensor of the covariant derivative is a map $\mathsf{T} : T\mathscr{B} \times T\mathscr{B} \to T\mathscr{B}$ by $\mathsf{T}(u,v) = \nabla_u v - \nabla_v u - [u,v]$. Writing, $\mathsf{T} = \mathsf{T}^a_{bc} dx^b \otimes dx^c \otimes \partial_a$,*

$$\mathsf{T}^a_{bc} = \Gamma^a_{bc} - \Gamma^a_{cb}, \tag{65}$$

*where $[u,v]$ is the Lie bracket of vector fields given by $(u^a \partial_a v^b - v^a \partial_a u^b) e_b$.*

**Definition A.3 (Curvature).** *The Riemannian curvature tensor is a map $\mathsf{R} : T\mathscr{B} \times T\mathscr{B} \times T\mathscr{B} \to T\mathscr{B}$ defined by $\mathsf{R}(u,v)w = \nabla_u \nabla_v w - \nabla_v \nabla_u w - \nabla_{[u,v]} w$. Writing $\mathsf{R} = \mathsf{R}^a_{bcd} \partial_a = R(\partial_c, \partial_d)\partial_b$,*

$$\mathsf{R}^a_{bcd} = \partial_c \Gamma^a_{db} - \partial_d \Gamma^a_{cb} + \Gamma^a_{ce} \Gamma^e_{db} - \Gamma^a_{de} \Gamma^e_{cb}, \quad \text{then } \mathsf{R}^a_{bcd} = -\mathsf{R}^a_{bdc}. \tag{66}$$

**Remark A.4.** *Curvature and torsion tensors are characteristics of the manifold, the existence of torsion and curvature tensors does not require the existence of a metric on the manifold $\mathscr{B}$.*

Consider now a metrisable manifold $\mathscr{B}$ endowed with covariant derivative $\nabla$ and a metric $\mathsf{g}$, the covariant derivative $\nabla$ is said to be *metric compatible* if and only if $\nabla \mathsf{g} = 0$ where

$$\Big(\nabla_v \mathsf{g}\Big)(u,w) = v\big[\mathsf{g}(u,w)\big] - \mathsf{g}(\nabla_v u, w) - \mathsf{g}(u, \nabla_v w). \tag{67}$$

In a coordinate system, this constraint imposes

$$\big(\nabla_c \mathsf{g}\big)_{ab} = \partial_c \mathsf{g}_{ab} - \Gamma^d_{ca} \mathsf{g}_{db} - \Gamma^d_{cb} \mathsf{g}_{da} = 0. \tag{68}$$

In this case, $(\mathscr{B}, \mathsf{g}, \nabla)$ is a RC manifold.

Let $v$ be a tangent vector to an arbitrary curve. Let us consider two vectors $u$ and $w$ obtained by parallel transport along the curve, then $\nabla_v u = 0$ and $\nabla_v w = 0$. In a RC manifold the inner product between them remains constant along the curve: $\nabla_v \mathsf{g}(u,w) = 0$. More generally, for any vector set $(u,v,w)$:

$$\nabla_v\big(\mathsf{g}(u,w)\big) = \mathsf{g}(\nabla_v u, w) + \mathsf{g}(u, \nabla_v w).$$

### A.2. Technical proofs

**Proof of formula** (16)**.** First, $v := \phi_* V = (F_A^a V^A)\partial_a$ a tangent vector to $\mathscr{B}$ at the point $x = \phi(X)$. Second, applying the ambient Ehresmann connection $n$, there is a unique horizontal lift $v^\uparrow = n(y)v = v^a\partial_a - n_a^i v^a \partial_i$ as a tangent vector to $T\mathscr{B}$ at $(x = \phi(X), y = \underline{\delta}F(X)\vartheta\, Y)$. Finally, the natural lift of $V$ is obtained by solving Equation (16), straightforward computations, using $\Omega_a^J = 0$, give

$$\begin{aligned} V^\uparrow &= \Omega_a^B v^{\uparrow a}\partial_B + \Omega_i^B v^{\uparrow i}\partial_B + \Omega_a^J v^{\uparrow a}\partial_J + \Omega_i^J v^{\uparrow i}\partial_J \\ &= \Omega_a^B F_A^a V^A \partial_B + \Omega_a^J F_A^a V^A \partial_J - \Omega_i^J n_a^i F_A^a V^A \partial_J \\ &= F_a^B F_A^a V^A \partial_B + \Omega_a^J F_A^a V^A \partial_J - \Omega_i^J n_a^i F_A^a V^A \partial_J \\ &= V^A \partial_A - \big(\Omega_i^J n_a^i F_A^a - \Omega_a^J F_A^a\big) V^A \partial_J. \end{aligned}$$

From this we can claim that the connection coefficients are

$$N_A^J = \Omega_i^J n_a^i F_A^a - \Omega_a^J F_A^a.$$

Finally, because $\Omega_Z^i \Omega_a^Z = \Omega_B^i \Omega_a^B + \Omega_J^i \Omega_a^J = 0$, one has $\Omega_J^i N_A^J = -\Omega_J^i \Omega_a^J F_A^a + \Omega_J^i \Omega_j^J n_a^j F_A^a = \Omega_B^i \Omega_a^B F_A^a + n_a^i F_A^a = \Omega_A^i + n_a^i F_A^a$. Once again, writing $\Omega_J^z \Omega_z^I = \Omega_J^a \Omega_a^I + \Omega_J^i \Omega_i^I = \Omega_J^i \Omega_i^I = \delta_J^I$, the connection can be rewritten in the form

$$N_A^I = \Omega_i^I \Omega_J^i N_A^J = \Omega_i^I \Omega_A^i + \Omega_i^I n_a^i F_A^a.$$

Using the notation $\Omega_i^I(X, Y) = \Theta_i^I(X)$ introduced in Section 3, formula (16) is verified. □

**Proof of formula** (26)**.** Let us compute the general form of the non-metricity tensor by computing separately each contribution of $\partial_A \mathtt{G}_{IJ} - \Gamma_{AI}^K \mathtt{G}_{KJ} - \Gamma_{AJ}^K \mathtt{G}_{IK}$:

$$\begin{aligned} \partial_A \mathtt{G}_{IJ} &= \partial_A \Big(\Theta_I^i \mathtt{g}_{ij} \Theta_J^j\Big) \\ &= \big(\partial_A \Theta_I^i\big)\mathtt{g}_{ij}\Theta_J^j + \Theta_I^i \mathtt{g}_{ij}\big(\partial_A \Theta_J^j\big) + \Theta_I^i \partial_A \mathtt{g}_{ij} \Theta_J^j. \end{aligned}$$

Keep in mind that, on the Euclidean space, the connection is metric compatible:

$$\begin{aligned} \partial_A \mathtt{g}_{ij} &= \delta_i^a \delta_j^b \partial_A \mathtt{g}_{ab} = \delta_i^a \delta_j^b \partial_c \mathtt{g}_{ab} F_A^c = \delta_i^a \delta_j^b \Big(\gamma_{ca}^d \mathtt{g}_{db} + \gamma_{cb}^d \mathtt{g}_{da}\Big) F_A^c \\ &= \Big(\gamma_{ai}^k \mathtt{g}_{kj} + \gamma_{aj}^k \mathtt{g}_{ki}\Big) F_A^a. \end{aligned}$$

Hence, one obtains

$$\begin{aligned} \partial_A \mathtt{G}_{IJ} &= \partial_A \Big(\Theta_I^i \mathtt{g}_{ij} \Theta_J^j\Big) \\ &= \big(\partial_A \Theta_I^i\big)\mathtt{g}_{ij}\Theta_J^j + \Theta_I^i \mathtt{g}_{ij}\big(\partial_A \Theta_J^j\big) + \Theta_I^i \Big(\gamma_{ai}^k \mathtt{g}_{kj} + \gamma_{aj}^k \mathtt{g}_{ki}\Big) F_A^a \Theta_J^j, \end{aligned}$$

$$\begin{aligned} \Gamma_{AI}^K \mathtt{G}_{KJ} &= \Theta_i^K\big((1-\zeta)\partial_A F_I^i + \zeta \partial_A \Theta_I^i\big)\Theta_K^k \mathtt{g}_{kj}\Theta_J^j \\ &\qquad + \Theta_k^K \gamma_{ai}^k F_I^i F_A^a (\Theta_K^l \mathtt{g}_{lj}\Theta_J^j) && \Theta_i^K \Theta_K^k = \delta_i^k \\ &= \delta_i^k\big((1-\zeta)\partial_A F_I^i + \zeta \partial_A \Theta_I^i\big)\mathtt{g}_{kj}\Theta_J^j + \gamma_{ai}^k F_I^i F_A^a \mathtt{g}_{kj}\Theta_J^j \\ &= \big((1-\zeta)\partial_A F_I^i + \zeta \partial_A \Theta_I^i\big)\mathtt{g}_{ij}\Theta_J^j + \gamma_{ai}^k F_I^i F_A^a \mathtt{g}_{kj}\Theta_J^j, \end{aligned}$$

$$\begin{aligned} \Gamma_{AJ}^K \mathtt{G}_{IK} &= \Gamma_{AJ}^K \mathtt{G}_{KI} && \mathtt{G}_{IK} = \mathtt{G}_{KI} \\ &= \big((1-\zeta)\partial_A F_J^i + \zeta \partial_A \Theta_J^i\big)\mathtt{g}_{ij}\Theta_I^j + \gamma_{ai}^k F_J^i F_A^a \mathtt{g}_{kj}\Theta_I^j && i \leftrightarrow j \\ &= \Theta_I^i \mathtt{g}_{ij}\big((1-\zeta)\partial_A F_J^j + \zeta \partial_A \Theta_J^j\big) + \gamma_{aj}^k F_J^j F_A^a \mathtt{g}_{ki}\Theta_I^i, \end{aligned}$$

$$
\begin{aligned}
\mathsf{Q}_{IJA} &= \big(\partial_A \Theta^i_I\big)\mathrm{g}_{ij}\Theta^j_J + \Theta^i_I \mathrm{g}_{ij}\big(\partial_A \Theta^j_J\big) - ((1-\zeta)\partial_A F^i_I + \zeta \partial_A \Theta^i_I)\mathrm{g}_{ij}\Theta^j_J - \\
&\qquad \Theta^i_I \mathrm{g}_{ij}((1-\zeta)\partial_A F^j_J + \zeta \partial_A \Theta^j_J) \\
&\qquad + \Big(\Theta^i_I\Big(\gamma^k_{ai}\mathrm{g}_{kj} + \gamma^k_{aj}\mathrm{g}_{ki}\Big)F^a_A\Theta^j_J - \gamma^k_{ai}F^i_I F^a_A \mathrm{g}_{kj}\Theta^j_J - \gamma^k_{aj}F^j_J F^a_A \mathrm{g}_{ki}\Theta^i_I\Big) \\
&= (1-\zeta)\Big(\big(\partial_A \Theta^i_I\big)\mathrm{g}_{ij}\Theta^j_J + \Theta^i_I \mathrm{g}_{ij}\big(\partial_A \Theta^j_J\big)\Big) \\
&\qquad - (1-\zeta)\Big(\partial_A F^i_I \mathrm{g}_{ij}\Theta^j_J + \Theta^i_I \mathrm{g}_{ij}\partial_A F^j_J\Big) \\
&\qquad + \Big(\gamma^k_{ai}\mathrm{g}_{kj}F^a_A\Theta^j_J(\Theta^i_I - F^i_I) + \gamma^k_{aj}\mathrm{g}_{ki}F^a_A\Theta^i_I(\Theta^j_J - F^j_J)\Big) \\
&= (1-\zeta)\mathrm{g}_{ij}\Big(\Theta^j_J\partial_A\big(\Theta^i_I - F^i_I\big) + \Theta^i_I\partial_A\big(\Theta^j_J - F^j_J\big)\Big) \\
&\qquad\qquad + \gamma^k_{ai}\mathrm{g}_{kj}F^a_A\Big(\Theta^j_J(\Theta^i_I - F^i_I) + \Theta^j_I(\Theta^i_J - F^i_J)\Big).
\end{aligned}
$$

Now the formula (26) is obtained by specialising $\mathrm{g}_{ij} = \delta_{ij}$ and $\gamma^k_{ai} = 0$. □

**Proof of formula** (32)**.** Recall the definition (32): $V^\uparrow = N(Y)V = \mathcal{H}^* n(y) v$ where $v^\uparrow = n(y)v = v^a\partial_a - n^i_a v^a \partial_i$ with $v = \phi_* V = F^a_A V^A \partial_A$. Using (31), straightforward computations give

$$
\begin{aligned}
V^\uparrow &= \mathcal{H}^B_a {v^\uparrow}^a \partial_B + \mathcal{H}^B_i {v^\uparrow}^i \partial_B + \mathcal{H}^J_a {v^\uparrow}^a \partial_J + \mathcal{H}^J_i {v^\uparrow}^i \partial_J \\
&= F^B_a v^a \partial_B + \mathcal{H}^J_a v^a \partial_J + \mathcal{H}^J_i {v^\uparrow}^i \partial_J \\
&= F^B_a F^a_A V^A \partial_B + \mathcal{H}^J_a F^a_A V^A \partial_J - \mathcal{H}^J_i n^i_a F^a_A V^A \partial_J \\
&= \delta^B_A V^A \partial_B - (\mathcal{H}^J_i n^i_a F^a_A - \mathcal{H}^J_a F^a_A) V^A \partial_J \\
&= V^A \partial_A - (\mathcal{H}^J_i n^i_a F^a_A - \mathcal{H}^J_a F^a_A) V^A \partial_J.
\end{aligned}
$$

Hence, the connection coefficients are

$$
N^J_A = \mathcal{H}^J_i n^i_a F^a_A - \mathcal{H}^J_a F^a_A.
$$

Next, as $\mathcal{H}^i_Z \mathcal{H}^Z_a = \partial_B \Psi^i F^B_a + \partial_I \Psi^i \partial_a \Psi^I = 0$, one obtains

$$
\begin{aligned}
\partial_I \Psi^i N^I_A =& \partial_I \Psi^i \big(\partial_j \Psi^I n^j_a F^a_A - \partial_a \Psi^I F^a_A\big) \\
=& \partial_I \Psi^i \partial_j \Psi^I n^j_a F^a_A + \partial_B \Psi^i F^B_a F^a_A \\
=& \partial_I \Psi^i \partial_j \Psi^I n^j_a F^a_A + \partial_A \Psi^i.
\end{aligned}
$$

Once again, because $\mathcal{H}^z_I \mathcal{H}^J_z = \mathcal{H}^a_I \mathcal{H}^J_a + \mathcal{H}^i_I \mathcal{H}^J_i = \mathcal{H}^i_I \mathcal{H}^J_i = \partial_I \Psi^i \mathcal{H}^J_i = \delta^J_I$, one obtains

$$
\begin{aligned}
N^J_A = \mathcal{H}^J_i \partial_I \Psi^i N^I_A &= \mathcal{H}^J_i \partial_I \Psi^i \partial_j \Psi^I n^j_a F^a_A + \mathcal{H}^J_i \partial_A \Psi^i \\
&= \partial_j \Psi^J n^j_a F^a_A + \partial_i \Psi^J \partial_A \Psi^i.
\end{aligned}
$$

This completes the proof. □